Critical role of the pore domain in the cold response of TRPM8 channels identified by ortholog functional comparison

Received for publication, February 2, 2018, and in revised form, May 30, 2018 Published, Papers in Press, June 7, 2018, DOI 10.1074/jbc.RA118.002256

María Pertusa[1], **Bastián Rivera, Alejandro González, Gonzalo Ugarte, and Rodolfo Madrid**

From the Departamento de Biología, Facultad de Química y Biología, and Millennium Nucleus of Ion Channels-Associated Diseases (MiNICAD), Universidad de Santiago de Chile, 9160000 Santiago, Chile

Edited by Roger J. Colbran

In mammals, the main molecular entity involved in innocuous cold transduction is TRPM8. This polymodal ion channel is activated by cold, cooling compounds such as menthol and voltage. Despite its relevance, the molecular determinants involved in its activation by cold remain elusive. In this study we explored the use of TRPM8 orthologs with different cold responses as a strategy to identify new molecular determinants related with their thermosensitivity. We focused on mouse TRPM8 (mTRPM8) and chicken TRPM8 (cTRPM8), which present complementary thermosensitive and chemosensitive phenotypes. Although mTRPM8 displays larger responses to cold than cTRPM8 does, the avian ortholog shows a higher sensitivity to menthol compared with the mouse channel, in both HEK293 cells and primary somatosensory neurons. We took advantage of these differences to build multiple functional chimeras between these orthologs, to identify the regions that account for these discrepancies. Using a combination of calcium imaging and patch clamping, we identified a region encompassing positions 526–556 in the N terminus, whose replacement by the cTRPM8 homolog sequence potentiated its response to agonists. More importantly, we found that the characteristic cold response of these orthologs is due to nonconserved residues located within the pore loop, suggesting that TRPM8 has evolved by increasing the magnitude of its cold response through changes in this region. Our results reveal that these structural domains are critically involved in cold sensitivity and functional modulation of TRPM8, and support the idea that the pore domain is a key molecular determinant in temperature responses of this thermo–transient receptor potential (TRP) channel.

Cold sensing is fundamental for the rapid initiation of physiological and behavioral thermoregulatory responses to drops in environmental temperature. In mammals, cold is detected by cold thermoreceptor neurons whose somas are located within trigeminal and dorsal root ganglia (1–3). The free nerve endings of these neurons express a variety of transduction and voltage-dependent ion channels that shape their electrical response elicited by cold temperatures. In this process, TRPM8 plays a critical role as a key molecular entity responsible for innocuous cold transduction (4–6). This protein belongs to the family of transient receptor potential (TRP)[2] ion channels, of which another 10 thermosensitive channels have been identified: TRPV1–4, TRPA1, TRPM2–5 and TRPC5 (reviewed in Refs. 7–9). TRPM8 is activated by cold and by cooling agents such as menthol and icilin (10, 11), it displays weak voltage dependence (12–14), and it has a key role not only in cold sensing but also in cancer and pathological cold-induced pain (reviewed in Refs. 15–17).

Functional TRPM8 channels are homotetramers (18–21), with cytosolic N and C termini and six transmembrane domains (TMs), where the interaction between TM5, TM6, and the pore loops conforms the permeation pathway (21). Within the six TMs most of the residues known to be involved in agonist and antagonist effects, and in voltage activation, have been mapped (20, 22–25). Although there is evidence of an important role of the C-terminal domain in the temperature dependence of TRPM8 (26, 27), and that specific residues within the transmembrane domains and the N terminus alter thermal responses (25, 28, 29), the molecular determinants of cold sensitivity of this thermo-TRP channel are not completely elucidated.

The fact that TRP channels are modular proteins, where mutations can selectively ablate one of the responses without altering the others, has led to the identification of regions or amino acids involved in TRPM8 activation by menthol or icilin, using high-throughput mutagenesis and analysis of chimeric proteins (22, 24). In this scenario, building chimeras using related cold-insensitive family members could represent a decent strategy for finding new molecular determinants involved exclusively in the cold response. Unfortunately, TRP channels have a weakly conserved protein sequence, and replacement experiments often yield non-

This work was supported by Fondo Nacional de Ciencia y Tecnología (FONDECYT) Grants 11130144 (to M.P.) and 1161733 (to R.M.), by the University of Santiago de Chile through the Dirección de Investigación, Científica y Tecnológica (DICYT) Grant 021843PP (to M.P.), and by the Iniciativa Científica Milenio through the Núcleo Milenio de Enfermedades Asociadas a Canales Iónicos (MiNICAD), funded by the Ministry of Economy, Development and Tourism, Chile. This work was also supported by the Comisión Nacional de Investigación Científica y Tecnológica (CONICYT) PhD Fellowship, Grant 21161660 (to B.R.). The authors declare that they have no conflicts of interest with the contents of this article.

[1] To whom correspondence should be addressed. Tel.: 56-2-271-82-955; E-mail: maria.pertusa@usach.cl.

[2] The abbreviations used are: TRP, transient receptor potential; TMs, transmembrane domains; DRG, dorsal root ganglia; CSN, cold-sensitive neurons; c, chicken; m, mouse; x, *Xenopus*; r, rat; P-helix, pore helix; MHR, melastatin homology regions; ANOVA, analysis of variance.

functional chimeras (22, 25, 29, 30), a problem that could be avoided by using orthologs. Evolutionary adaptation drives species-specific differences in channel properties, and using highly conserved TRP orthologs to construct chimeras usually generates functional channels, where it is possible to identify relevant protein domains (24, 30–35). Orthologs of TRPM8 have been found in tetrapods but not in bony fish or invertebrates (36). Although all characterized TRPM8 channels from different species retain cold sensitivity, there are major differences in temperature and menthol activation between *Xenopus laevis* (xTRPM8), *Rattus norvegicus* (rTRPM8), and *Gallus gallus* (cTRPM8) (24, 37), suggesting that nonconserved regions could be involved in these disparities.

Considering that chicken and mouse TRPM8s share an identity of 79.9%, and taking advantage of their different thermosensitive and chemosensitive phenotypes, we constructed a variety of chimeras with the final goal of identifying key molecular determinants associated with cold detection. Our results reveal that positions within the pore loop contribute to TRPM8 cold activation, and that residues within the proximal N-terminal domain are critical for fine-tuning this polymodal thermoTRP channel function.

Results

Chicken TRPM8 displays lower cold responses compared with the mouse ortholog

The chicken TRPM8 ortholog (cTRPM8) was first characterized in a study where its insensitivity to icilin was exploited to identify the residues involved in the activation of rat TRPM8 (rTRPM8) by this compound (24). The same study also reported higher sensitivity of cTRPM8 to menthol compared with the murine ortholog. Although it was suggested that cTRPM8 has a greater sensitivity to cold (24, 37), the cold-induced response of cTRPM8 channels has not been studied in further detail.

To characterize the responses of mouse and chicken TRPM8 channels to cold and menthol, we used a combination of calcium imaging and patch clamp techniques. Taking advantage that TRPM8 is a Ca^{2+}-permeable nonselective cation channel (10, 11), we first used calcium imaging to compare the cold-induced responses of these orthologs in intact cells, a well-established noninvasive approach to study this channel (10, 11, 25, 29, 38–40). HEK293 cells expressing cTRPM8 or mTRPM8 were exposed sequentially to a cold ramp, to a 100 μM menthol pulse, and to a saturating stimulus where a second cold ramp in the presence of this chemical agonist was applied to elicit the maximal channel response (Fig. 1*A*). We found that mTRPM8-transfected cells displayed a large cold-induced response and a menthol-evoked response at 34 °C that correspond to nearly 60% of the maximal response (Fig. 1*A*, *left panel*; Fig. 1*B*). Conversely, in cTRPM8-transfected cells, the amplitude of the cold response represented less than 50% of the maximum, whereas menthol application was enough to obtain a response equivalent to the saturating one (Fig. 1*A*, *right panel*; Fig. 1*B*). To further characterize cTRPM8 channels, we compared the temperature threshold and the menthol sensitivity of cells expressing both TRPM8 orthologs. To achieve this, we used an extended protocol consisting of a cold ramp followed by the application of increasing menthol concentrations (from 3 to 300 μM), ending with a final cold ramp in the presence of 300 μM menthol (Fig. 1*C*). The resulting concentration-response curves show that cTRPM8-expressing cells are more sensitive to menthol at lower concentrations than mTRPM8(+) cells, with an estimated EC_{50} of 117 ± 12 μM for mTRPM8 and 19 ± 3 μM for cTRPM8 (Fig. 1*D*). In contrast, the cumulative population of cTRPM8-expressing cells recruited during a cold ramp (*i.e.* percent of the successfully transfected cells activated at a given temperature) show a significant shift in the curve toward lower temperatures compared with mTRPM8 cells (Fig. 1*E*). Notice that at the temperature that recruits 50% of cTRPM8-expressing cells, nearly 98% have been recruited at the same temperature in mTRPM8. In these experiments, the mean temperature threshold of mTRPM8(+) cells was 26.9 ± 0.2 °C, whereas in cells transfected with cTRPM8 this value was 23.1 ± 0.2 °C (Student's *t* test, $p < 0.001$), suggesting that the lower cold-induced response observed in the avian channel is related to lower thermal sensitivity of cells expressing cTRPM8. It is important to note that the temperature threshold is an operational parameter that corresponds to the temperature at which a significant increase in the current or fluorescence of a given cell is observed. It does not imply that these channels must overcome a temperature value to open, because the open probability is a smooth function of the temperature (12, 13).

Although Ca^{2+} imaging is a powerful tool to study TRPM8 function, this is not necessarily a linear readout of channel activity. To further explore the mechanism that could explain the functional differences observed in both orthologs using a more direct approach, we performed patch clamp experiments. Under whole-cell configuration, transfected HEK293 cells were held at −60 mV and channel activation was probed with voltage ramps from −100 to +180 mV at 0.2 Hz, to obtain their respective I–V relationships. Cells were stimulated using the same protocol as in calcium imaging experiments (*i.e.* sequential applications of cold, menthol at 34 °C, and cold in the presence of menthol) (Fig. 1*F*). In tight correlation with the calcium imaging results, cells expressing cTRPM8 exhibited smaller cold-evoked currents and larger responses to 30 μM menthol than mTRPM8 cells (Fig. 1, *G* and *H*). Cold and menthol activation of TRPM8 is linked to a shift of the voltage-activation curve toward more negative (physiologically relevant) membrane potentials (12, 13, 38). To estimate the voltage at 50% of activation ($V_{1/2}$) and the maximal conductance (g_{max}), the current traces derived from the voltage ramps were fitted with a Boltzmann-linear function (see "Experimental Procedures") (41). As observed in Fig. 1*I*, the differences in the responses to cold and menthol displayed by cTRPM8 compared with mTRPM8 can be explained by differences in the $V_{1/2}$ of activation. Compared with the results obtained with the murine ortholog, in the cold condition the estimated $V_{1/2}$ value is significantly shifted toward a more positive membrane potential (Fig. 1*I*). Additionally, during menthol stimulation this parameter is 50 mV more negative in the avian ortholog, indicating that in cTRPM8 channels menthol exerts a more important effect than cold temperatures. The lack of differences between

maximal conductance values (Fig. 1*J*), suggests that the disparity observed between these orthologs could be explained mainly by differences in the gating mechanism.

To characterize the cold-induced response in more detail, we also evaluated how the current developed during a cold ramp. When the current at +100 mV was normalized to the maximal current obtained during the temperature drop (cold at 20 °C), the relative increase in chicken and mouse channels did not present major differences (Fig. 1*K*, *upper panel*). However, it is noteworthy that when these values were normalized to the maximal response of the channel induced by menthol at 20 °C (*i.e.* cold plus menthol stimulus), the current at the lowest temperature is close to 40% of the maximal response observed in mTRPM8 cells, and only 10% of that observed in cTRPM8 cells (Fig. 1*K*, *lower panel*). This observation indicates that although the current variation during a cold drop is similar between both channels, there is an important difference in the proportion that the cold-induced response represents compared with the

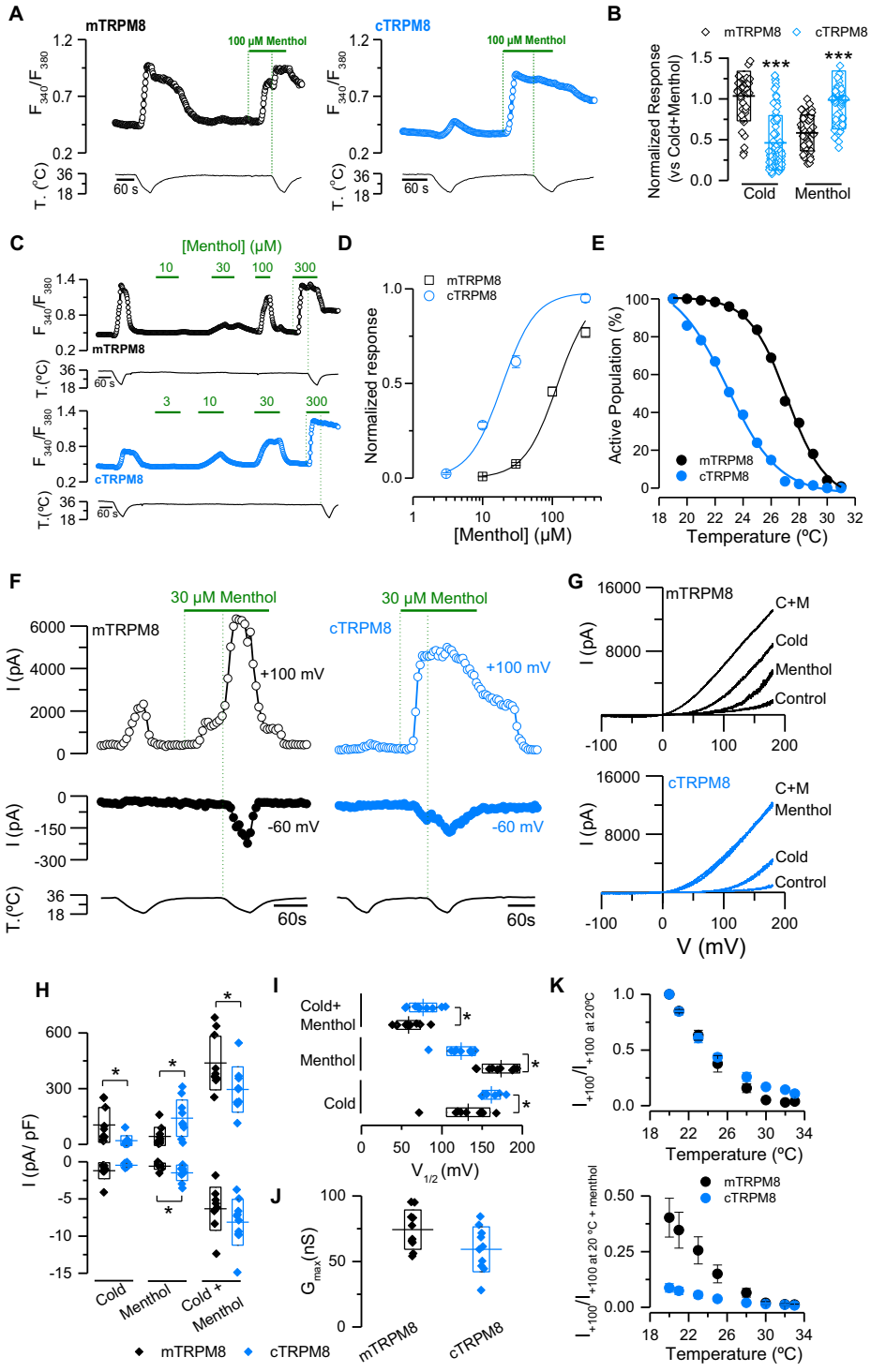

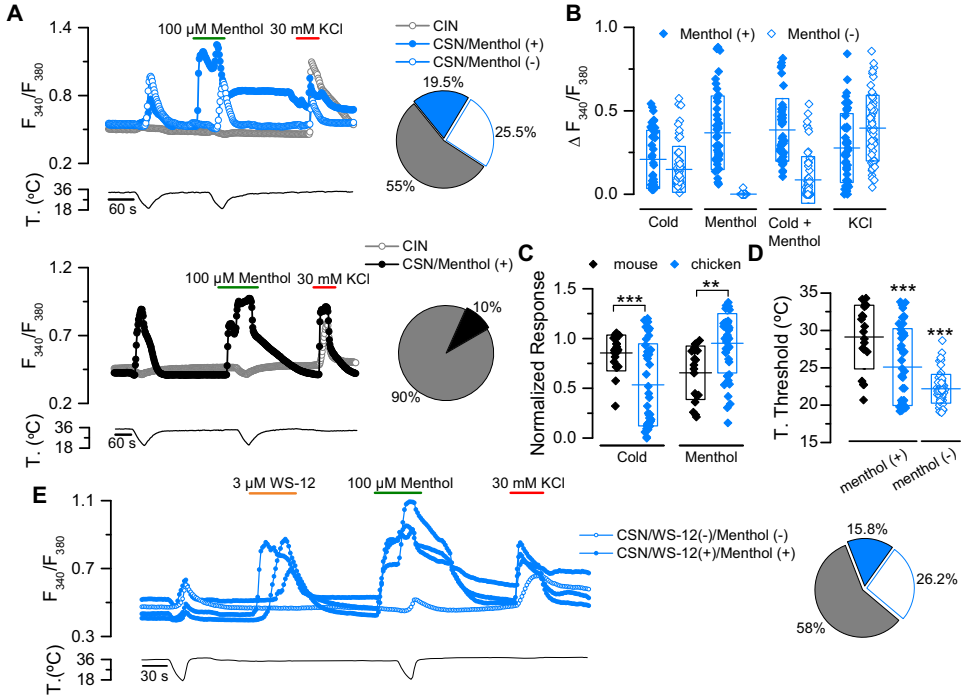

Figure 2. Native cTRPM8 displays both smaller cold-induced responses and higher menthol-induced responses than mTRPM8. *A*, ratiometric $[Ca^{2+}]_i$ response of representative cold-sensitive/menthol-sensitive neurons (*CSN/Menthol* (+)), cold-sensitive/menthol-insensitive neurons (*CSN/Menthol* (−)), and cold-insensitive neurons (*CIN*) from chicken (*upper panel*) and mouse (*bottom panel*) DRG neurons. The protocol used consisted of a cooling ramp, followed by application of 100 μM menthol at 34 °C, followed by a cold ramp in the presence of the chemical activator, and finally depolarization induced by 30 mM KCl. The pie plots on the *right* summarize the percentages of each subpopulation. *B*, scatter plot with mean ± S.D. of the responses to cold, menthol, cold+menthol, and KCl of Menthol (+) and Menthol (−) CSNs from chicken DRG neurons (cCSNs/Menthol (+) $n = 45$, and cCSNs/Menthol (−) $n = 59$). *C*, scatter plot with mean ± S.D. of cold- and menthol-induced responses normalized to the maximal response (cold plus menthol) of chicken and mouse CSN/Menthol (+) neurons. Statistical significance was assessed with an unpaired Student's *t* test. **, $p < 0.01$; ***, $p < 0.001$; mCSN/Menthol (+) $n = 19$, cCSN/Menthol(+) $n = 45$. *D*, mean temperature threshold of cold-sensitive neurons from chicken and mouse DRGs (mCSN/Menthol (+), $n = 19$ (*black*), cCSN/Menthol (+), $n = 45$ (*blue*), and cCSN/Menthol (−), $n = 59$ (*white*)). Statistical significance was assessed by an ANOVA in combination with a Bonferroni's post hoc test: ***, $p < 0.001$. *E*, ratiometric $[Ca^{2+}]_i$ response of representative cold-sensitive/WS-12-sensitive/menthol-sensitive (*CSN/WS-12* (+)/*Menthol* (+)) and cold-sensitive/WS-12-insensitive/menthol-insensitive (*CSN/WS-12* (−)/*Menthol*(−)) neurons from chicken DRG neurons. The pie plot on the *right* summarizes the percentages of each subpopulation (cCIN, $n = 83$ (*gray*); cCSN/WS-12 (+)/Menthol (+), $n = 23$ (*blue*) and cCSN/WS-12(−)/Menthol (−), $n = 38$ (*white*)).

maximal current elicited by a cold plus menthol stimulus in both orthologs. Thus, we hypothesized that the nonconserved amino acids of TRPM8 between chicken and mouse orthologs are behind the differences observed in cold and menthol responsiveness.

Differential cold- and menthol-induced responses of cTRPM8 channels are conserved in native membranes

Previous studies have shown that the menthol-induced response exhibited by cTRPM8 is larger than mTRPM8 (24, 37, 42). However, the finding that the cold-induced response is considerably lower in cTRPM8 is completely novel. To rule out that this observation was the result of the expression system used to characterize the cTRPM8-dependent response, we performed the same experiments analyzing TRPM8 native channels in chicken and mouse dorsal root ganglia (DRG) neurons.

When characterizing cold-sensitive neurons (CSNs) from chicken DRG, we observed two important differences compared with mouse neurons. First, in chicken DRG nearly 45% of the neurons responded to temperature drops compared with only 10% observed in mouse DRG (Fig. 2*A*). Second, and in agreement with a previous report (42), we observed that a large percentage of CSNs are menthol-insensitive. This population, as shown in Fig. 2, *A* and *B*, is comprised of neurons that

Figure 1. Differential responses to cold and menthol in cTRPM8 compared with mTRPM8. *A*, representative ratiometric $[Ca^{2+}]_i$ traces showing responses of HEK293 cells transfected with mTRPM8 (*black*) and cTRPM8 (*blue*) to cold, 100 μM menthol, and a combined stimulus of cold in the presence of 100 μM menthol. *Upper trace* shows $[Ca^{2+}]_i$ and lower trace represents bath temperature. In this study, *green vertical dotted lines* indicate the start of menthol and cold + menthol stimuli. *B*, scatter plot with mean ± S.D. Individual values were normalized to the maximal response of the cells in the cold plus menthol condition. Statistical significance was assessed with an unpaired Student's *t* test: ***, $p < 0.001$; mTRPM8, $n = 45$; cTRPM8, $n = 91$. *C*, time course of $[Ca^{2+}]_i$ in HEK293 cells transfected with mTRPM8 and cTRPM8. *D*, menthol concentration-response curves at 34 °C in transfected HEK293 cells (mTRPM8, $n = 77$; cTRPM8, $n = 51$). Responses were normalized to the amplitude obtained with maximal stimulation (300 μM menthol plus cold). *E*, percentage of the active population, defined as the fraction of cells that are positively transfected and whose apparent temperature threshold exceeds the temperature at that point, recruited during a cooling ramp in HEK293 cells transfected with mTRPM8 ($n = 122$) or cTRPM8 ($n = 142$). *F*, representative recording of whole-cell currents measured at +100 and −60 mV in HEK293 cells transfected with mTRPM8 or cTRPM8 channels. *G*, current–voltage relationships of mTRPM8 and cTRPM8 at 34 °C in control solution (*Control*), at 20 °C in control solution (*Cold*), menthol at 34 °C (*Menthol*), and menthol at 20 °C (*Cold + Menthol*). *H–J*, scatter plot with mean ± S.D. of all values corresponding to the maximal current density at +100 and −60 mV (*H*), $V_{1/2}$ values (*I*), and g_{max} estimated in the cold + menthol condition (*J*). *K*, relative currents of mouse and chicken TRPM8 at +100 mV during a cold pulse. In the *upper panel*, the values are normalized to $I_{+100\,mV}$ at 20 °C; in the *bottom panel*, they are normalized to $I_{+100\,mV}$ at 20 °C during menthol application. Recordings from mouse and chicken TRPM8 were always interlaced on the same day. Statistical significance was assessed with a two-tailed unpaired Student's *t* test: *, $p < 0.05$; ***, $p < 0.001$; $n > 5$ cells for each condition.

respond to cold but are unresponsive to menthol at 34 °C, and do not exhibit potentiation of cold-induced responses in the presence of this chemical agonist. This observation suggests that in contrast to mouse primary somatosensory neurons, where virtually all CSNs are also menthol-sensitive (43, 44), TRPM8 is not the main molecular entity underlying cold transduction in *G. gallus* DRG neurons.

In agreement with our previous observations using the recombinant system, when we compared the responses of cold- and menthol-sensitive neurons from mouse and chicken DRG cultures, we found that the normalized cold response was lower in avian neurons compared with the mouse cells, but chicken CSNs (cCSNs) exhibited higher responses to this cooling compound than mouse CSNs (mCSNs) (Fig. 2*C*). Moreover, we also observed that the smaller cold-induced responses of cCSNs also correlated with a shift in the temperature threshold toward lower temperatures. The mean temperature threshold of mCSNs was around 29 °C; in chicken TRPM8(+) neurons, this value was ~25 °C, and close to 22 °C in menthol-insensitive neurons (Fig. 2*D*), similar to the values reported by Yamamoto *et al*. (42). To corroborate that cold- and menthol-sensitive neurons identified in chicken DRG cultures express TRPM8, we performed the same protocol as in Fig. 2*A* adding an application of WS-12, a more specific TRPM8 agonist than menthol (45). We observed similar populations of menthol-sensitive and menthol-insensitive CSNs in these experiments (Fig. 2*E*), compared with those reported previously (Fig. 2*A*). Remarkably, all the menthol-sensitive CSNs neurons also responded to WS-12, suggesting that the cold- and menthol-sensitive neurons in chicken DRG cultures are TRPM8(+). Thus, our results in DRG neurons suggest that native and recombinant cTRPM8 display both smaller cold-induced responses and higher menthol responses than mTRPM8. In this scenario, the strategy to construct chimeras using both orthologs represents an opportunity to identify molecular determinants related with the TRPM8 cold response.

Transfer of chicken transmembrane domains to mTRPM8 rendered a chimera with a cTRPM8 phenotype

We designed a set of three chimeras, where the N-terminal, transmembrane core, and C-terminal domains were replaced by the chicken ortholog sequence, as depicted in Fig. 3*A*. Because differences in the sequence between these two species are important, and to detect protein expression levels of different channels with a unique (and efficient) antibody, the Myc epitope was added in the C-terminal domain, including the WT channels (mM8-myc, cM8-myc). We previously reported that the incorporation of this epitope does not modify TRPM8 activity (29). As observed in Fig. 3, all three chimeras showed different responses to those exhibited by mM8-myc channels. The chimera where the N-terminal domain was exchanged (N-tercM8+mM8-myc) shows an unexpected new phenotype compared with mouse and chicken orthologs. This chimeric channel displayed higher responses to cold and menthol, along with a shift of 4 °C in the thermal threshold to higher temperatures (Fig. 3, *B–E*), suggesting that the N-terminal part of cTRPM8 contains sequences that could enhance the thermal and chemical responses of mTRPM8. In contrast, the construct that has the C-terminal domain of cTRPM8 (C-tercM8+mM8-myc) displayed a small reduction in responses to cold and menthol stimuli (Fig. 3, *B–E*). Interestingly, the chimera containing the N- and C-terminal domains from mTRPM8, and part of pre-TM1 and the transmembrane core domains of cTRPM8 (pre-TM1+6TMcM8+mM8-myc) accurately replicates the phenotype of cTRPM8, suggesting that the characteristic behavior displayed by the avian ortholog is related to amino acids located in this part of the protein.

The pore domain contains residues involved in the cold-induced response of TRPM8

Next, we sought to identify the molecular determinants that account for the responses to cold and menthol displayed by the pre-TM1+6TMcM8+mM8-myc chimera. For this, we compared the responses of new constructs where six transmembrane domains (6TMcM8+mM8-myc) or only the pore domain (porecM8+mM8-myc) of mM8-myc were replaced by the cTRPM8 sequence. Ca^{2+} imaging experiments showed that the 6TMcM8+mM8-myc chimera displayed a similar phenotype to that exhibited by the cTRPM8 channel (Fig. 4*A*), suggesting that the transmembrane core domain is largely responsible for the functional behavior of the chicken ortholog. However, the chimera that only contains the pore domain (*i.e.* transmembrane domain 5 and 6 and the connecting loop) of the cTRPM8 (porecM8+mM8-myc) displayed a mixed phenotype, characterized by a reduced cold response along with an increase in the activation temperature threshold. In contrast to cTRPM8, this chimera showed a menthol response similar to mM8-myc (Fig. 4*A*). These results suggest that the molecular determinants involved in the characteristic responses of cTRPM8 to cold and menthol could be distributed in different regions of the avian ortholog. Thus, amino acids within the pore domain seem to be related to the lower response to cold, whereas part of the high sensitivity to menthol is probably caused by differences in residues located within the first four transmembrane domains. Regarding the cold response, amino acid sequence alignment between mouse and chicken TRPM8 revealed that the main differences are concentrated in the pore loop. If these residues are indeed behind the reduced cold response displayed by chicken TRPM8, the exchange of the pore loop of cTRPM8 by mTRPM8 should generate a version of the chicken channel with an enhanced response to thermal stimulus. As predicted, compared with cM8-myc, the resulting chimera (loopmM8+cM8-myc) did not show alterations in menthol sensitivity, but exhibited an important increase in the cold-induced response, suggesting that residues within this domain can alter the activation of TRPM8 channel by cold (Fig. 4, *B–E*).

Next, we tried to identify the specific amino acids that are responsible for these particular cold responses. This region exhibited 84.2% sequence identity. Considering that these differences are spread throughout the whole loop, we constructed two chimeras: ½loopN-tercM8+mM8-myc and ½loopC-tercM8loop+ mM8-myc (see Fig. 4, *A* and *B*). The phenotype of these two mutants showed that modifications in the first part of the pore loop have a major impact on the cold response; compared with mM8-myc, ½loopN-tercM8+mM8-myc

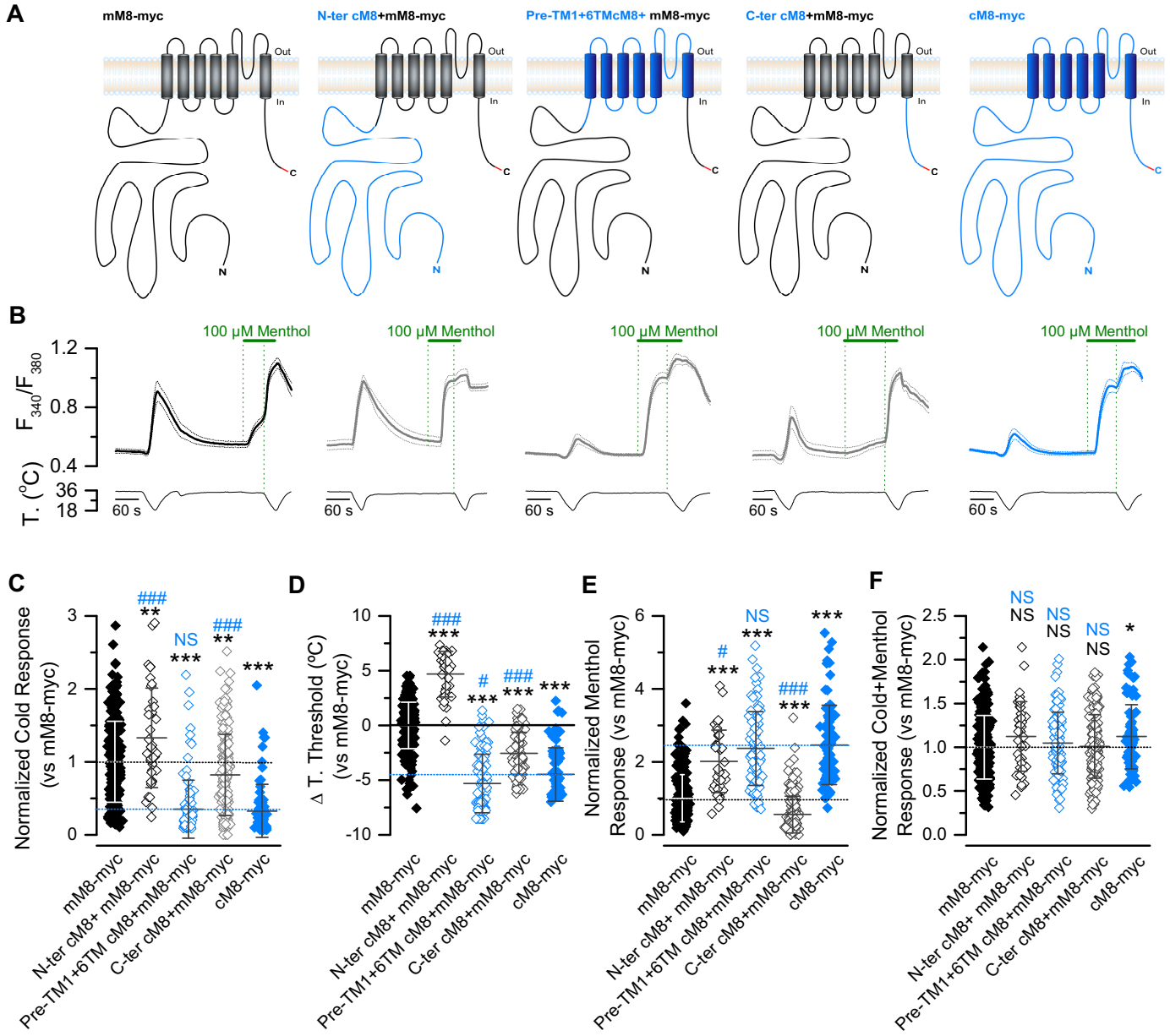

Figure 3. The functional behavior of the cTRPM8 channel is not related with the residues in its cytosolic domains. *A*, schematic representation of chimeric channels. The sequences from cTRPM8 are colored in *blue*, and the sequences from mTRPM8 in *black*. The presence of the Myc epitope in the C-terminal domain is highlighted in *red*. *B*, average (*solid line*) ± S.E. (*dotted lines*) time course of $[Ca^{2+}]_i$ level (F_{340}/F_{380}) in HEK293 cells ($n > 15$ cells in each case) transfected with mM8-myc (*black*), chimeric channels (*gray*), and cM8-myc (*blue*). *C–F*, Scatter plot with mean ± S.D. of cold- (*C*), menthol- (*E*), and cold + menthol–induced responses (*F*) of TRPM8 orthologs and chimeras. The values were normalized to the mean response observed in mM8-myc (control condition) in parallel experiments. (mM8-myc, $n = 253$; N-ter cM8+mM8-myc, $n = 38$; pre-TM1+6TMcM8+mM8-myc, $n = 105$; C-ter cM8+mM8-myc, $n = 165$; cM8-myc, $n = 78$.) Mean shift in temperature threshold displayed by each mutant is expressed according to the mM8-myc values. Positive values indicate shifts toward warmer temperatures (*D*). In *A–C*, statistical significance was assessed by an ANOVA test in combination with a Dunnett's post hoc test: *, $p < 0.05$; **, $p < 0.01$; ***, $p < 0.001$, compared with mM8-myc; #, $p < 0.05$; ###, $p < 0.001$ to cM8-myc; *NS*, not significant.

showed an ~70% reduction, however, the ½loopC-tercM8+mM8-myc construct only displayed an 18% (Fig. 4, *C–E*). Comparing the mouse and chicken sequences of the N-terminal portion of the pore loop (see below in Fig. 7), we observed differences at four residues. One of the differences that caught our attention was the change in charge displayed by positions Glu-887 in cTRPM8 and Arg-897, its homologous position in the mouse ortholog. Considering that this glutamate is also found in TRPM8 from *X. laevis* (see Fig. 7), whose cold responses have also been reported as smaller compared with murine orthologs (37), we thought that this change could at least partially account for the differences we observed. In fact, the responses of the point mutant R897E in mM8-myc also showed a decreased response to cold, temperature threshold values below those in mM8-myc, and unaltered menthol responses (Fig. 4, *B–E*). Altogether, these results suggest that nonconserved pore loop residues are key molecular determinants behind the differences in the cold response exhibited by mouse and chicken TRPM8 orthologs.

To study in detail whether sensitivity to menthol is also altered in cells that expressed the chimeric versions of the channel with exchanged loops (loopcM8+mM8-myc and loopmM8-cM8-

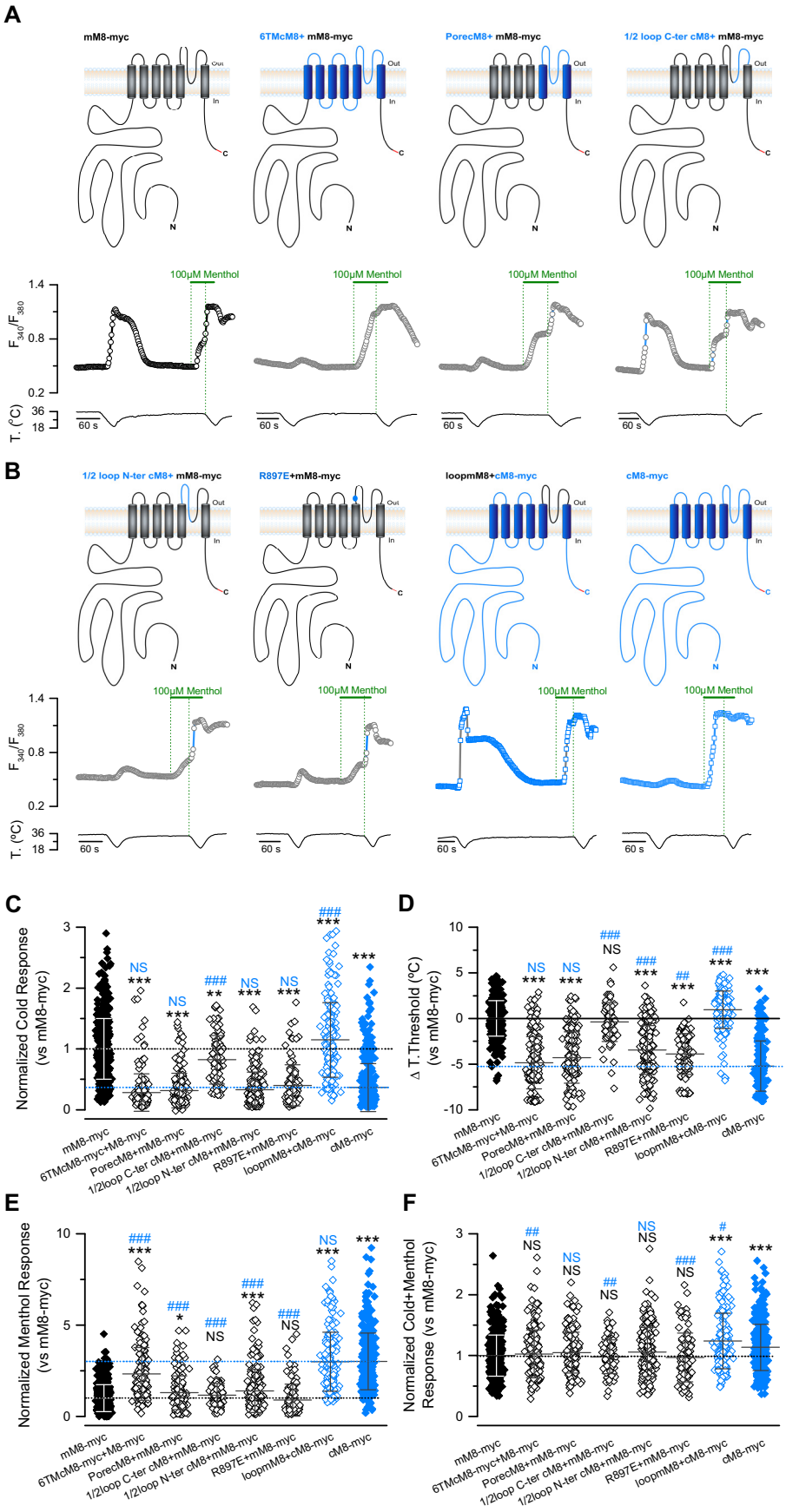
A
mM8-myc
6TMcM8+ mM8-myc
PorecM8+ mM8-myc
1/2 loop C-ter cM8+ mM8-myc
100µM Menthol
F340/F380
T. (°C)
60 s
B
1/2 loop N-ter cM8+ mM8-myc
R897E+mM8-myc
loopmM8+cM8-myc
cM8-myc
C
Normalized Cold Response (vs mM8-myc)
D
Δ T.Threshold (°C) (vs mM8-myc)
E
Normalized Menthol Response (vs mM8-myc)
F
Normalized Cold+Menthol Response (vs mM8-myc)
mM8-myc
6TMcM8-myc+M8-myc
PorecM8+mM8-myc
1/2loop C-ter cM8+mM8-myc
1/2loop N-ter cM8+mM8-myc
R897E+mM8-myc
loopmM8+cM8-myc
cM8-myc

myc) (Fig. 5*A*), we used the same protocol as that used in Fig. 1*E* to estimate both temperature threshold and EC_{50} to menthol (Fig. 5*B*). The relationship between these two parameters is plotted in Fig. 5*C* for each construct and WT channels (mM8-myc and cM8-myc). When the values of loopcM8+mM8-myc chimera and mM8-myc are compared, the 3 °C difference in temperature threshold, it is not translated into changes in the EC_{50} value (mM8-myc: 127 ± 6 μM *versus* loop cM8+mM8-myc 115 ± 11 μM; $p > 0.05$, unpaired *t* test). A similar observation arises when the values of loopmM8+cM8-myc chimera and cM8-myc are compared: a large shift of 3.5 °C in the temperature threshold was observed (Fig. 5*C*) with no alterations in menthol sensitivity (EC_{50} cM8-myc: 34 ± 3 μM *versus* loop mM8+cM8-myc 40 ± 2 μM; $p > 0.05$, unpaired *t* test). However, it is important to mention that although the exchange of the pore loop induces a considerable thermal shift, it is not enough to achieve complete transformation in terms of temperature threshold. The statistical analysis shows that this value is different when chimeras and the WT channel corresponding to the pore loop sequence are compared (Fig. 5*C*), suggesting that, although this domain concentrates amino acids with a critical contribution to the differences in cold responses of these two orthologs, other regions of the protein could also be involved.

As previously shown in Fig. 1*I*, the differences in cold and menthol responses exhibited by mouse and chicken TRPM8 are related to differential shifts in the $V_{1/2}$ values. To corroborate that the same mechanism could underlie the altered cold response observed in the pore loop chimeras, we performed patch clamp experiments. As shown in Fig. 5, *D* and *E*, and in agreement with calcium imaging results, when normalized whole-cell currents from the WT channel and the loop construct are compared, significant alterations in their cold-induced responses were observed, with no differences in their menthol-evoked currents. As expected, this change in the cold response is due to a shift in the $V_{1/2}$ of ~50 mV toward more negative membrane potentials in the case of loopmM8-cM8-myc *versus* cM8-myc, and toward more positive values comparing loopcM8-mM8-myc *versus* mM8-myc (Fig. 5*F*). Remarkably, this shift is observed only in cold-induced responses, whereas the $V_{1/2}$ in menthol remains unaltered, reinforcing the idea that cold responses can be affected without changes in menthol sensitivity.

From our results, it is clear that the cold response elicited by temperature drops from 35 to 20 °C in TRPM8 channels is strongly influenced by nonconserved amino acids within the pore loop. Nevertheless, are these residues also related to the thermosensitivity of the channel? In other words, is the 10-degree temperature coefficient (Q_{10}) different between these channels? To answer this question, we determined the Q_{10} (see "Experimental Procedures") of these four constructs (Fig. 5*G*). Using Equation 2, this value was obtained from the slope of the log(*I*) *versus T* plot (Fig. 5*G*, *upper panel*), where a highly temperature-dependent regime can be observed between 29 and 22 °C in all these channels. Estimation of the Q_{10} did not show differences between the four constructs (Fig. 5*G*, *lower panel*). This suggests that because thermosensitivity appears to be similar, other factors such as how the thermosensor is coupled to the gating of the channel could be altered.

Residues within the proximal N-terminal region tune the sensitivity of TRPM8 to cold and menthol

Although the pore loop contains amino acids that are critically involved in cold-induced responses of TRPM8, other regions of the channel could also be relevant for its final response to cold and/or menthol (26, 29, 46, 47). As shown in Fig. 3, we observed that the N-terminal chimera (N-tercM8+mM8-myc, henceforth 693) presents an increased response to cold and menthol, suggesting that the N-terminal part of cTRPM8 contains sequences that enhance mTRPM8 function. To identify the region responsible for this phenotype, we generated chimeras 556, 507, and 360, where the numbers indicate the extension of the N-terminal domain that was exchanged (Fig. 6*A*, *left panel*). Compared with 693, whose functional behavior in calcium imaging is shown in Fig. 6*A* (*right panel*), only chimera 556 showed the same enhanced responses to cold and menthol, along with a shift of 4 °C in the temperature threshold (Fig. 6, *A–D*). These results suggest that the sequence responsible for this increase in TRPM8 function is located within the region encompassing positions 507 and 556. In fact, responses displayed by the 507–556 construct demonstrate that this assumption was correct (Fig. 6, *A–D*). Within this 50–amino acid region, the first 20 residues are highly conserved, whereas the differences are concentrated in the last 30 residues, as shown in Fig. 7*A*.

To narrow down the sequence that determines functional behavior, we designed the chimeras 507–546 and 546–556. These constructs showed an intermediate and complementary phenotype (Fig. 6, *A–D*). Although 507–546 displays an enhanced response to menthol, it shows no increase in the cold-induced response. Conversely, 546–556 showed higher potentiation of its cold responsiveness but moderate increases in menthol-induced responses. Moreover, the shift in the temperature threshold of these two chimeras is around 1.5 °C, far from the almost 4 °C displayed by the 507–556 chimera, suggesting that the meaningful portion of this behavior is spread throughout this particular 30 amino acid region (Fig. 6, *A–D*).

To further characterize the agonist sensitivity of the different chimeric TRPM8 channels, we examined their temperature threshold and their concentration response to menthol using the extended protocol (Fig. 6*E*). In contrast to mM8-myc, cells

Figure 4. The small cold-induced response of cTRPM8 compared with mTRPM8 is because of residues in the pore loop. *A* and *B*, *upper panels*, schematic representation of the chimeric channels. Sequences from cTRPM8 are colored in *blue*, and sequences from mTRPM8 in *black*. The Myc epitope in the C-terminal domain of the channels is highlighted in *red*. A representative intracellular Ca^{2+} trace (F_{340}/F_{380}) of each construct is shown below each channel. *C–F*, mean responses to cold (*C*), menthol (*E*), and cold plus menthol (*F*) of TRPM8 orthologs, chimeras, and mutants characterized in this part of the study. The values were normalized to the mean response observed in mM8-myc (control condition) in parallel experiments; mM8-myc, $n = 524$; 6TMcM8+mM8-myc, $n = 187$; porecM8+mM8-myc, $n = 176$; ½loop N-ter cM8+mM8-myc, $n = 207$; ½loop C-ter cM8+mM8-myc, $n = 86$; R897E+mM8-myc, $n = 110$; loopmM8+cM8-myc, $n = 198$; cM8-myc, $n = 391$. In *D*, scatter plot with mean ± S.D. shows the temperature threshold shift displayed by each mutant expressed according to the mM8-myc values. Positive values indicate shifts to warmer temperatures. Statistical significance was assessed by an ANOVA test with a Dunnett's post hoc test: *, $p < 0.05$; **, $p < 0.01$; ***, $p < 0.001$ to mM8-myc; #, $p < 0.05$; ##, $p < 0.01$; ###, $p < 0.001$ to cM8-myc; *NS*, not significant.

expressing 507–556 were more sensitive to cold and menthol (Fig. 6, *F* and *G*). Whole-cell patch clamp experiments corroborate the results obtained through Ca^{2+} imaging experiments, where a marked increase in the amplitude of the response to agonists is observed in cells transfected with the 507–556 chimera (Fig. 6, *H–J*). In the particular case of this chimera, the enhanced responses to agonists is both related to a shift in the voltage dependence curve of ~30 mV toward more negative membrane potentials (Fig. 6*K*), and to an important increase in maximal conductance (g_{max}) (Fig. 6*L*). This change in g_{max}

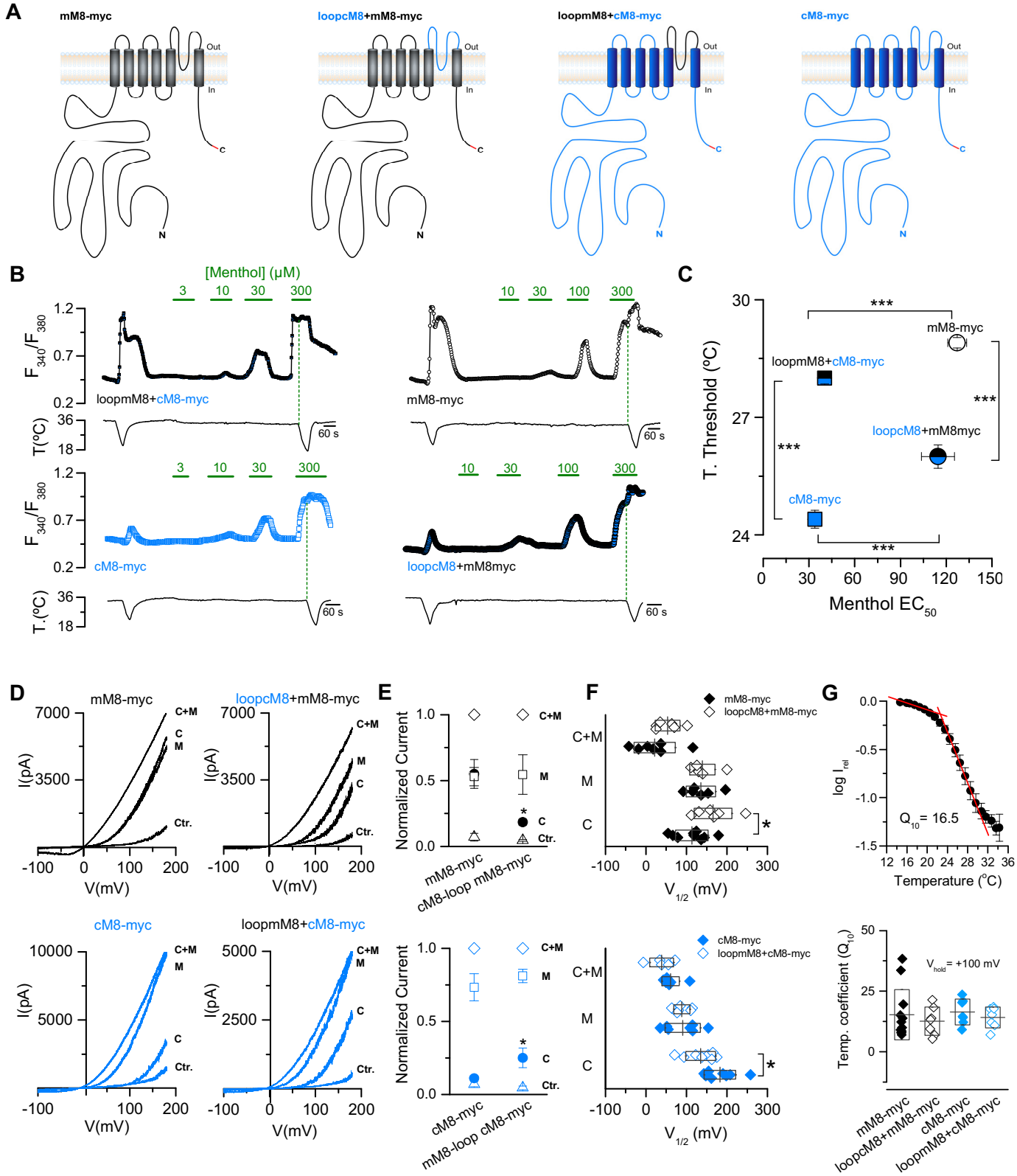

could be explained by a higher number of channels at the cell surface. As shown in Fig. 6*M*, this was not related to an increased expression level of this construct, because whole protein extracts of HEK293 cells transfected with mM8-myc and 507–556 chimera revealed similar amounts of TRPM8 protein. Therefore, this result suggests that this particular region could play a role in recruiting mTRPM8 channels in the plasma membrane. To further support these observations, we also estimated the number of both channels at the cell surface using nonstationary noise analysis (39, 48) (Fig. 6*N*). Using this approach, we observed an important increase in the number of active channels in cells that expressed the 507–556 construct; we counted 1209 ± 128 channels in contrast to 617 ± 62 channels displayed by cells expressing mM8-myc ($n_{\text{mM8-myc}} = 8$, $n_{507-556} = 6$; two-tailed unpaired Student's *t* test: **, $p < 0.01$). Unitary conductance, estimated from the mean single channel unitary current for the WT and mutant channel at 19 °C, was ~50 picosiemens in both cases, similar to the values reported previously for TRPM8 WT channels (13, 39). Thus, we have also identified a region within the N-terminal proximal domain of cTRPM8 whose transference to mTRPM8 enhanced channel function, increasing the number of channels in the plasma membrane and producing a shift in the voltage activation curve toward physiologically relevant membrane potentials.

Discussion

TRP channels are polymodal, responding to multiple stimuli, including exogenous chemical ligands, lipids, voltage, and, in the case of thermo-TRP channels, temperature. Mutation experiments have demonstrated that is possible to ablate one of their modalities without altering their responses to other stimuli (22, 26, 30, 33, 49–51); suggesting that different stimuli use distinct activation pathways that finally result in channel opening. Our attempts to unveil the molecular basis underlying cold sensitivity of TRPM8 channels, led to the identification of the pore loop as a critical structural domain exclusively involved in its temperature-dependent response, and a 30 amino acid region within the proximal N terminus significantly contributing to their biophysical properties and trafficking.

One important question that has been intensively studied in the field of thermo-TRP channels is the structural basis of their temperature-dependent gating. Several studies have searched for the minimal structure of these tetramers required to elicit a cold or heat response and, therefore, determine whether there is a structural domain that works as a temperature sensor (reviewed in Ref. 52). It has been suggested that thermosensitivity in ion channels could be explained by specific residues that do not necessarily conform a specialized domain (53, 54). Over the past years, an important number of studies have focused on dissecting the structural parts related to the temperature-dependent gating of some thermo-TRPs, revealing that regions or amino acids within the N-terminal domain (30, 31, 33, 51, 55, 56) or the pore domain (49, 50, 57, 58) are involved in this process. However, most of these findings are linked to heat-sensitive TRPs. In TRPM8, mutagenesis studies have revealed that the C-terminal domain (26, 27), and the residues Arg-842 and Lys-856 (25) are involved in its cold sensitivity, with these two amino acids also contributing to its gating charge and menthol response (25).

The phenotype exhibited by the pore chimeras we used in this study showed major alterations in their cold responses without displaying significant changes in their activation by menthol, suggesting that part of the cold-activation process is unique and depends, at least partially, on the structure of the pore loop. However, the fact that the analysis of the Q_{10} values of mTRPM8, cTRPM8, and the pore chimeras did not reveal important differences, this led us to speculate that the pore loop is not part of the putative thermosensor, but probably plays a role in how the change in its conformation is transmitted to finally open the channel in response to a temperature drop. Nevertheless, it is important to emphasize that the parameters that are indeed physiologically relevant, such as the amplitude of the cold response in a defined range and the cell temperature threshold, are indeed tightly dependent on which of these channels the cell is expressing.

The pore loop can be dissected into three parts: A short TM5–P-helix linker, a pore helix (P-helix), and an extracellular linker P-helix–TM6 loop (21), where the location of the selectivity filter has been suggested (59, 60). Previous studies have shown that residues within this domain are important contributors to the TRPM8 function, but in contrast with the results presented here, where an exclusively and specific alteration of the cold response was observed, these molecular determinants affect temperature- and menthol-induced responses to the same extent. For instance, TRPM8 is *N*-glycosylated in the P-helix–TM6 loop on asparagine 934 (39, 61, 62), and this post-translational modification contributes to TRPM8 sensitivity to chemical and thermal stimuli (39). In a different study, rationalized point mutations identified at position Tyr-908, within the pore helix, nearly ablated the TRPM8 response to cold and menthol, without altering the icilin response, suggesting that this residue is important for cold- and menthol-dependent gating, but is not required to the same extent for icilin-induced

Figure 5. The pore loop of TRPM8 as a key molecular determinant of the distinctive cold-induced response of chicken and mouse orthologs. *A*, schematic representation of the constructs. *B*, time course of the $[Ca^{2+}]_i$ response in HEK293 cells transfected with these constructs. *C*, relationship of mean temperature activation thresholds and the EC_{50} to menthol for each construct (mM8-myc, $n = 123$; cM8-myc, $n = 144$; cM8loop+mM8-myc, $n = 72$; mM8loop+cM8-myc, $n = 139$). Statistical significance was assessed by an ANOVA in combination with a Bonferroni's post hoc test. ***, $p < 0.001$. In the case of the data displayed by the *blue* and *black square*, the size of the dot representing the mean value is bigger than S.E. *D*, current–voltage relationships obtained in HEK293 cells transfected with these four constructs at 34 °C in control solution (*Ctr.*), at 20 °C in control solution (*C*), at 34 °C with 100 μM menthol (*M*), and at 20 °C during a stimulus of 100 μM menthol (*C* + *M*). *E*, normalized values (to cold + menthol condition) of the currents obtained at +100 mV in the different conditions tested. *F*, scatter plot with mean ± S.D. of $V_{1/2}$ values. In *E* and *F*, experiments were performed in pairs: mM8-myc *versus* cM8loop-mM8-myc and cM8-myc *versus* mM8loop+cM8-myc. Statistical significance was assessed with a two-tailed unpaired Student's *t* test: *, $p < 0.05$; $n \geq 5$ cells for each condition. *G*, the *upper panel* shows the plot of log (*I*) *versus* temperature of cells transfected with mM8-myc; each point represents the average of 10 experiments. Cold-induced currents were measured at the end of 75 ms voltage steps from 0 to +100 mV (0.5 Hz) during a cold ramp from 35 to 15 °C. The *bottom panel* summarizes the Q_{10} values for each construct; $n = 7$–10 cells for each condition.

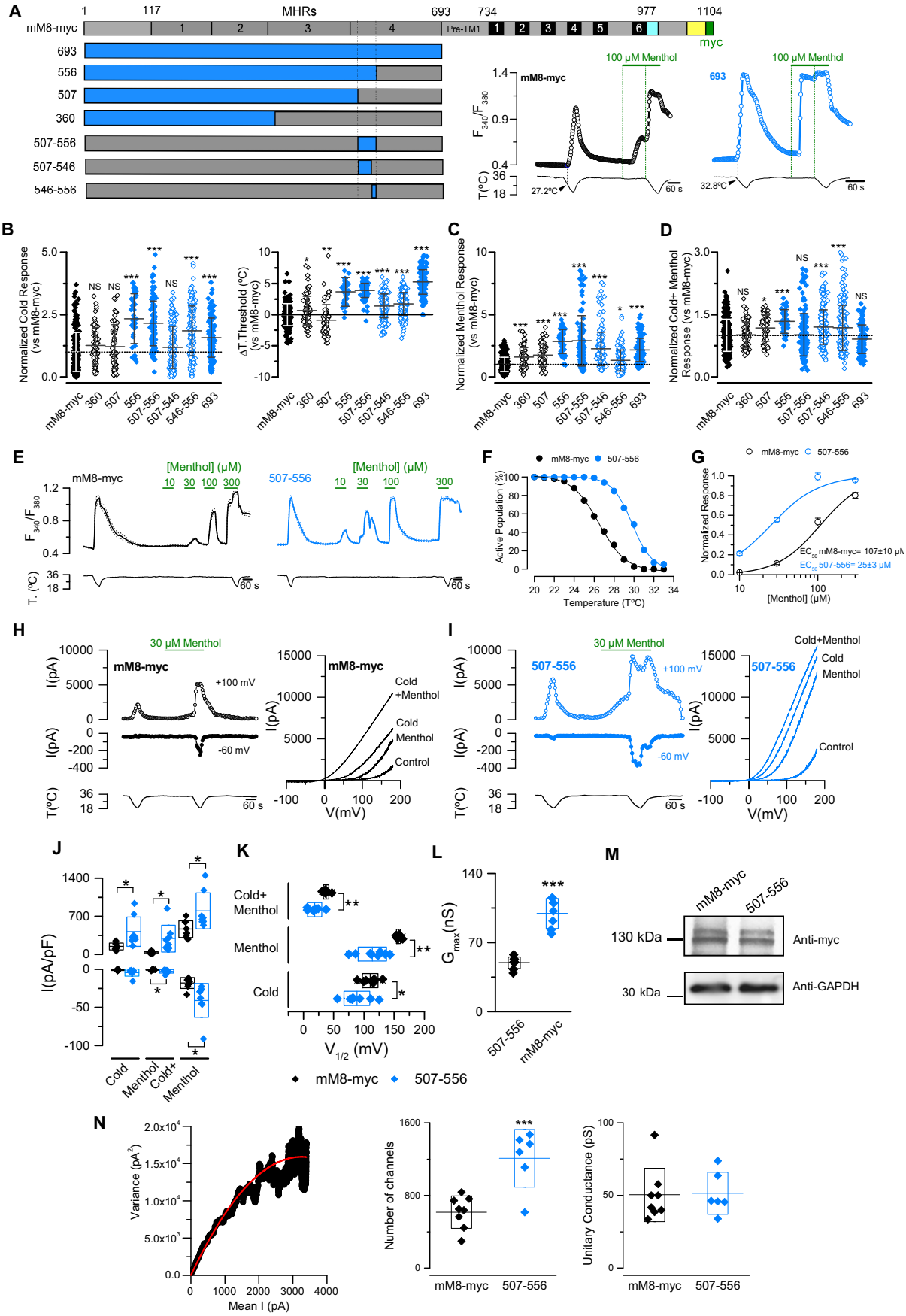
A
mM8-myc
MHRs
Pre-TM1
myc
693
556
507
360
507-556
507-546
546-556
100 μM Menthol
mM8-myc
693
B
Normalized Cold Response (vs mM8-myc)
ΔT.Threshold (°C) (vs mM8-myc)
C
Normalized Menthol Response (vs mM8-myc)
D
Normalized Cold+ Menthol Response (vs mM8-myc)
E
mM8-myc
507-556
[Menthol] (μM)
F
Active Population (%)
Temperature (T°C)
G
Normalized Response
[Menthol] (μM)
H
30 μM Menthol
mM8-myc
+100 mV
-60 mV
Cold +Menthol
Cold Menthol
Control
V(mV)
I
507-556
Cold+Menthol
J
I(pA/pF)
Cold
Menthol
Cold+ Menthol
K
V1/2 (mV)
L
Gmax (nS)
M
130 kDa
30 kDa
Anti-myc
Anti-GAPDH
N
Variance (pA²)
Mean I (pA)
Number of channels
Unitary Conductance (pS)

activation (60). Although the role of the pore domain as a molecular determinant in the cold-induced response of TRPM8 is still emerging, its contribution as a molecular determinant for temperature sensing in other thermo-TRP channels is known (49, 50, 57). In TRPV1, mutants at positions N628K, at the beginning of the P-helix, and at N652T and Y653T within the P-helix–TM6 linker reduce the current observed at 40 °C, because heat stimuli induce smaller shifts in the $V_{1/2}$ to more negative potentials in these mutants compared with WT channels (49), similar to our observations with pore chimeras. In TRPA1 channels, Gly-878 amino acid within the TM5 is the only molecular determinant identified that participates in the characteristic cold-dependent response of the murine orthologs (32). Our study shows that TRPM8 also belongs to the group of thermo-TRPs where part of the temperature activation is linked to amino acids that are within the pore, tempting us to speculate that conformational changes of this domain are required to specifically open the channel by a low temperature stimulus, similar to the temperature-dependent rearrangements proposed for TRPV1 (58, 63, 64).

Our mechanistic comprehension of how cold or menthol conveys the opening of TRPM8 is scarce. The recently published cryo-EM structure of the homotetrameric TRPM8 channel from a collared flycatcher (21) that exhibits a 94% identity with cTRPM8 represents a meaningful step toward unveiling the structures related to cold- and menthol-dependent TRPM8 gating. However, an important part of the pore loop is missing in the final model (21), making it difficult to speculate, in structural terms, about the contribution of these nonconserved amino acids to channel activation by cold. Nevertheless, TRPM8 cryo-EM structure highlights the difference exhibited by the architecture between the pores of TRPV1 and TRPM8. First, TRPM8 lacks the turret connecting TM5 and the pore helix, the position of the pore helix is located further away from the ion permeation pathway, and the P-helix–TM6 loop is much longer compared with TRPV1. Moreover, in contrast to other TRP channels, TRPM8 does not have non–α-helical elements (*e.g.* 3_{10} or π helices) and an obvious TM4–TM5 linker to provide helical bending points important for channel gating (21, 65–67). These differences emphasize that, although the pore is relevant in TRPV channels and TRPM8 to be activated by temperature, a direct translation from our current knowledge about the residues required to open other TRPV channels by temperature to TRPM8 channels could be misleading.

Regarding menthol activation, the functional phenotype of the different transmembrane chimeras we designed also indicates that the potentiation of the menthol response exhibited by the chicken ortholog is mainly related to a different part of the protein, specifically amino acids located within the sequence encompassing the first four transmembrane domains, where most of the positions responsible for menthol-dependent TRPM8 response have been mapped (20, 22, 23). Interestingly, the TRPM8 cryo-EM structure showed that TM1–TM4 conform a cavity where the Tyr-745, Arg-842, and Tyr-1005, residues involved in the activation of TRPM8 by menthol, are located. In this study, the authors proposed that this cavity could act as the binding site for menthol and menthol-like molecules (21). It is interesting to point out that the alignment of TM1–TM4 sequences of human, rat, mouse, and chicken TRPM8 (Fig. 7) reveals important differences between mammal channels, with an equivalent sensitivity to menthol (24, 29, 37, 68), compared with cTRPM8 (this study and Refs. 24, 37, and 42) characterized to display a remarkably lower EC_{50} to menthol. Moreover, xTRPM8, that exhibits reduced menthol sensitivity compared with the other orthologs (37), also displays important differences in the amino acid sequence of the same region compared with TRPM8 channels from mammals and chicken (Fig. 7*A*), suggesting that nonconserved amino acids within the TM1–TM4 are behind the different sensitivities displayed by these orthologs. Further studies using the TRPM8 structure will shed light if differences in these positions contribute to stabilizing the binding of menthol to TRPM8, or facilitate the conformational change required to open the channel by this agonist.

Our study also reveals the important contribution of the N-terminal domain to TRPM8 responses to cold and menthol. Although the N terminus of TRPM8 represents 66% of the subunit (residues 1 to 733), it has been scarcely studied, and only the 60 first residues have been reported to be involved in channel function and biogenesis (29, 46). The N terminus contains four melastatin homology regions (MHR) defined by the sequence similarity displayed by all the TRPM members (69). We found a stretch of 30 amino acids within the proximal

Figure 6. Transference of the proximal N-terminal domain of cTRPM8 to the murine ortholog produces an increase in its responses to cold and menthol. *A*, *upper horizontal bar*, primary structure of TRPM8. The TRP domain (in *cyan*), the coiled-coil region (in *yellow*), and the Myc epitope (in *green*) are depicted. *Lower horizontal bars*, schematic representation of N-terminal chimeras; sequences from cTRPM8 are colored in *blue*, and sequences from mTRPM8 in *gray*. On the *right*, representative time course of $[Ca^{2+}]_i$ in HEK293 cells transfected with mM8-myc (*black*) and 693 chimeric channels (*blue*) are shown. *B–D*, scatter plots with mean ± S.D. of the individual responses to cold (*B*), menthol (*C*), and cold + menthol (*D*) of TRPM8 N-terminal chimeras. The values were normalized to the mM8-myc mean response. (mM8-myc, $n = 239$; 360, $n = 79$; 507, $n = 63$; 556, $n = 45$; 693, $n = 125$; 507–556, $n = 114$; 507–546, $n = 195$; 546–556, $n = 195$). *Right panel* in *B* shows the shift in temperature threshold displayed by each mutant expressed according to the mM8-myc values. Statistical significance in *B–D* was assessed by an ANOVA test in combination with a Dunnett's post hoc test; *, $p < 0.05$; ***, $p < 0.001$, compared with mM8-myc. *E*, time course of $[Ca^{2+}]_i$ response in transfected HEK293 cells. *F*, percentage of active population recruited during a cooling ramp in positively transfected HEK293 cells (mM8-myc, $n = 157$; 507–556, $n = 256$). *G*, menthol concentration-response curves. The Hill equation fit yielded an EC_{50} of 107 ± 10 μM for mM8-myc ($n = 47$) and 25 ± 3 μM for 507–556 ($n = 50$). Responses were normalized to the amplitude obtained with maximal stimulation (300 μM menthol plus cold). *H* and *I*, *left panels*, representative whole-cell currents measured at +100 and −60 mV in HEK293 cells transfected with mM8-myc (*H*) and 507–556 (*I*). *Right panels* show current–voltage relationships for each condition: control, cold, 30 μM menthol, and cold + menthol. *J–L*, scatter plots with mean ± S.D. of the values of maximal current density at −60 and +100 mV (*J*), $V_{1/2}$ (*K*) and g_{max} values estimated in cold + menthol condition (*L*). Statistical significance was assessed with a two-tailed unpaired Student's *t* test: *, $p < 0.05$; $n > 6$ cells for each condition. *M*, Western blots of lysates from HEK293 cells transfected with mM8-myc and 507–556, probed with an anti-Myc antibody and anti-GAPDH as a loading control. *N*, *left panel*, dot plot of variance *versus* mean current obtained from whole-cell current of an HEK293 cell expressing mM8-myc channels. *Solid line* corresponds to the fit of the data to a parabola (Equation 3). *Right panels*, scatter plots with the mean ± S.D. of the number of active channels and unitary conductance, for both mM8-myc and 507–556. Statistical significance was assessed with a two-tailed unpaired Student's *t* test: ***, $p < 0.001$; $n \geq 6$ cells for each condition.

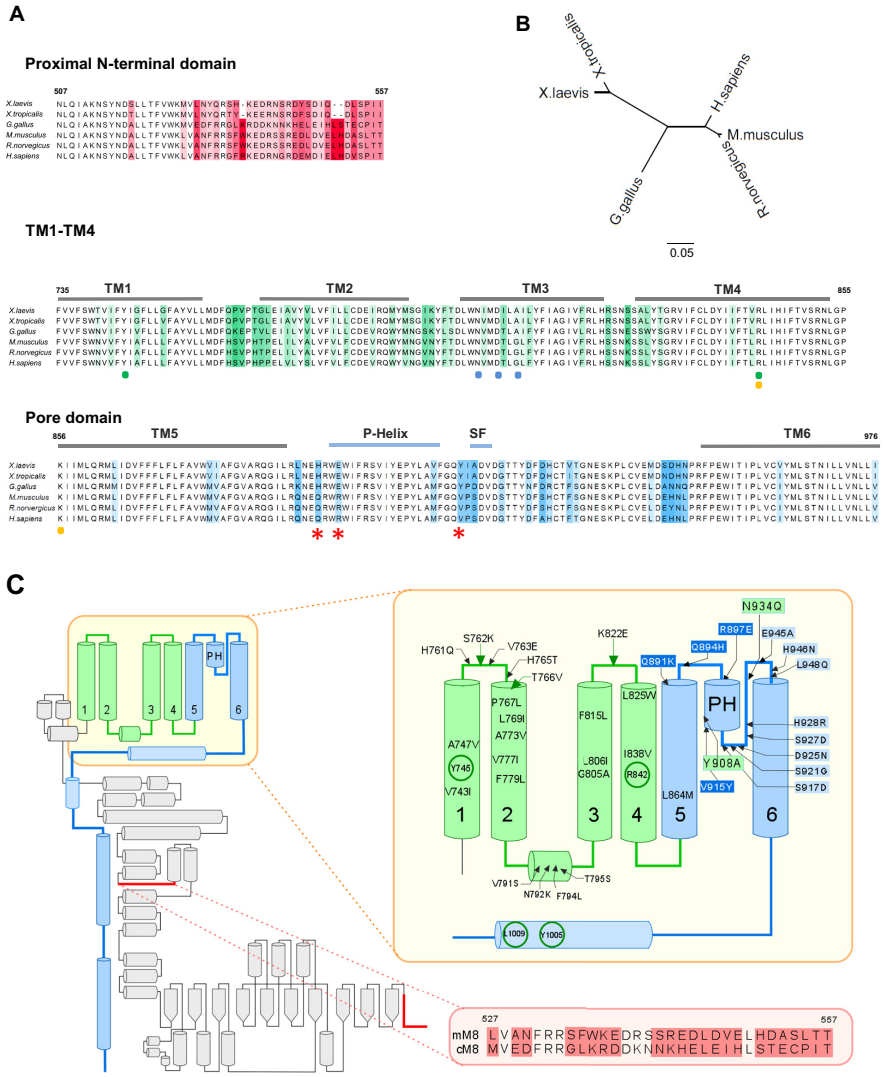

Figure 7. TRPM8 channels during vertebrate evolution. *A*, alignment of three different regions: proximal N-terminal domain (*upper panel*), TM1–TM4 domains (*central panel*), and the pore domain (*lower panel*), of *X. laevis*, *Xenopus tropicalis*, *G.gallus*, *R. norvegicus*, *Mus musculus*, and *Homo sapiens* orthologs of TRPM8 using ClustalW (76) and Jalview (77). Numbers correspond to residues in mTRPM8. *Red asterisks* indicate positions conserved in cTRPM8 and xTRM8 but not in mammal orthologs. *Dots* denote residues critical for the sensitivity of TRPM8 to menthol (*green*), icilin (*blue*), and voltage (*orange*). *B*, a phylogenetic tree was reconstructed with the neighbor-joining method (78) using MEGA7 (79) and FigTree v1.4.3. *C*, model of the TRPM8 subunit showing its secondary structure elements (modified from Ref. 21). The first four transmembrane domains involved in the potentiated menthol response of chicken TRPM8 and the TRP domain are colored in *green*, nonconserved positions between mouse and chicken are indicated. Critical residues for menthol sensitivity of TRPM8 channel are highlighted using a *green circle* (20, 22). Regions involved in the TRPM8 cold response are colored in *blue*: the C-terminal domain (26), and the pore domain (this study). Within the pore loop the nonconserved positions are highlighted in *dark blue* (N-terminal part) and *light blue* (C-terminal part). The *green squares* in Asn-934 and Tyr-908 positions indicate mutations that impact both the cold and menthol TRPM8 responses (39, 60). The distal and proximal N-terminal regions that influence general mechanisms of gating and trafficking are highlighted in *red* (29, 46) and this study). The *zoom-out* of the proximal N-terminal domain shows the detail of the sequence alignment were nonconserved positions are located. *Panel C* was modified from work that was originally published in Science. Yin, Y., Wu, M., Zubcevic, L., Borschel, W. F., Lander, G. C., and Lee, S.-Y. Structure of the cold- and menthol-sensing ion channel TRPM8. *Science*. 2018; 359:237–241. © the American Association for the Advancement of Science

region of the N-terminal domain that, in contrast to the pore loop, affects cold and menthol responses alike. This region that enhances TRPM8 function is located between two helix-turn-helix motifs in MHR4, and it is characterized by a low identity among TRPM8 orthologs (41%; see Fig. 7*A*), suggesting that this part of the protein could be involved, to some extent, in the species-specific functional differences observed in TRPM8. As we have previously shown, enhancement in responses to cold and menthol of the 507–556 chimera are because of alterations in the gating properties, but also an increase in channel expression at the plasma membrane. This was an unexpected effect considering that the WT cTRPM8 did not show similar differences in the g_{max} value compared with the mTRPM8. This could be because of the context provided by the mTRPM8 channel, where this inserted sequence enhances the ability of this region to modulate the channel's trafficking.

The required characterization of the WT orthologs performed in this study corroborates some aspects from previous reports and adds new important information. First, we observed that in both recombinant and native systems cells expressing cTRPM8 displayed a 3 °C higher temperature threshold compared with cells expressing the mouse ortholog. However, in a previous report, the estimation of the $T_{50\%}$ (the temperature that renders the half-maximal TRPM8 cold

response) of chicken, rat, and *Xenopus* (xTRPM8) orthologs was close to 30 °C in transfected cTRPM8 cells, 25 °C in cells expressing rTRPM8 and ~12 °C in xTRPM8-expressing cells. This could seem contradictory because if we assume that the $T_{50\%}$ of cTRPM8 is around 30 °C in the study performed by Myers *et al.* (37), the temperature threshold would probably be located above this value. In this regard, it has to be considered that these parameters could be dependent on the cellular context where the channels are expressed (39, 70). In the present study we used transfected HEK293 cells and DRG neurons to study recombinant and native channels, respectively, whereas Myers *et al.* (37) conducted their experiments in *Xenopus* oocytes. Second, we also reported a reduction in the magnitude of cold-induced currents of cTRPM8-expressing cells compared with the maximal response obtained under saturating costimulation with cold and menthol. In the electrophysiological characterization of mouse and chicken orthologs, we observed that normalized cold-induced current corresponded to 40% of the maximal current observed in mTRPM8, and only 10% in cTRPM8. Because the protocols used in other studies were not designed to apply a saturating stimulus of cold and menthol (37, 42), this striking difference could be overlooked.

Considering these findings, one important question that emerges is how this lower cold-induced response, observed at the molecular level, influences the avian thermal response. Yamamoto's study and ours characterized the cold responses of somatosensory neurons of chicken and mouse DRG. Consistently, both groups found a large proportion of cold-sensitive neurons in chicken DRG cultures. However, in contrast to that observed in mouse, only a fraction of this population responded to menthol, suggesting that other molecular entities besides TRPM8 have a role in chicken cold transduction. This other thermotransducer is not TRPA1, because it has been reported that cTRPA1 is not sensitive to cold but is activated by heat (34), and it has been also proposed that the thermal activation of menthol-insensitive neurons involves Ca^{2+} release from intracellular stores (42). In addition, despite the higher core temperature in birds compared with mice, the mean temperature threshold of the cold-sensitive neurons is as high as 23.5 °C, including both menthol-sensitive and menthol-insensitive neurons, and in our experiments only 10% of these neurons displayed temperature threshold values above 26 °C. This scenario is significantly different from the one described in mice, where ~10% of the neurons are cold-sensitive, most of them characterized as TRPM8(+), and ~75% of this population displaying a temperature threshold above the 26 °C in both trigeminal and spinal territories (43, 44). Because there is a tight correlation between the threshold for action potential firing and for $[Ca^{2+}]_i$ increases in each individual neuron (40, 71), these differences observed in the temperature threshold of the cold-sensitive neurons are extremely physiologically relevant, and reveal the existence of different neural and molecular determinants behind cold thermotransduction in chickens, and probably in multiple avian species. Considering the existence of other proteins that could be involved in cold detection such as TRPC5, voltage-gated and background K^+ channels, and voltage-gated Na^+ channels, among others (reviewed in Refs. 72–74), further studies are required to clarify this process in birds.

Endothermy is a fundamental event in vertebrate evolution that changed the dependence of animals on the environmental temperature. This property emerges from the acquisition of new mechanisms and the adaptation of existing ones associated with thermoregulation and thermosensitivity. In that regard, TRPM8 appears for the first time in amphibians and is present in reptiles, birds, and mammals. As shown in Myers' study, during evolution TRPM8 emerges as an ion channel that requires great drops in temperature to be robustly activated (37). In ectotherms such as reptiles and amphibians, it is likely that their free nerve endings undergo important changes in temperature, and therefore it is less necessary to have a channel that responds to small temperature drops. For birds, the residues within the pore loop that are responsible for the decrease in cTRPM8 cold responses are conserved in several avian species, and it is reasonable to speculate that the cold response of their TRPM8 channels could be similar. Although it could be difficult to conceal the high core body temperature of birds (over 40 °C) with the poor activation of cTRPM8 by the cold, the distinct nature of the neural and molecular mechanisms of cold sensing in birds could explain the relative contribution of this channel to avian cold transduction. In mammals on the other hand, innocuous cold thermotransduction is mainly carried out by TRPM8 (4–6). As endotherms, at room temperature conditions (22–23 °C), cold-sensitive nerve endings are exposed to ~33 °C at the skin, and in an extreme cold stimulus of −5 °C during 30 s, the intracutaneous temperature will be around 20 °C (75). Thus, a useful innocuous cold thermotransducer for mammals requires the ability of being robustly activated by cold temperatures just below 33 °C. This could explain how these changes in the pore domain may have been selected during evolution, because they make this channel relevant as a cold transducer in this range of temperatures. Interestingly, a recent report showed that 13-lined ground squirrels and Syrian hamsters, mammalian hibernators that have to withstand prolonged periods exposed to low temperatures, also have a poor cold activated version of TRPM8 (28). Analysis of chimeras of rat and squirrel TRPM8 orthologs revealed that the cold sensitivity displayed by rat TRPM8 can be re-introduced in the squirrel channel replacing homologous residues from the rat channel scattered within the core transmembrane domain (28). This study and ours support the idea that the setting of the TRPM8 cold response through evolution is intimately associated with changes within the transmembrane core domain of the protein, including the pore.

In conclusion, we identified two novel structural domains critically involved in TRPM8 function. The region encompassing positions 526 to 556 in the proximal N-terminal domain affects general mechanisms of gating and trafficking, and more importantly our report demonstrates that nonconserved residues between mouse and chicken orthologs of TRPM8 within the pore loop have a critical role in the cold-induced responses of TRPM8. Our results reinforce the notion that the cold activation process is unique, and support the idea that the pore domain is a key structural determinant in the temperature sensitivity of thermo-TRP channels.

Experimental procedures

Molecular biology, chimeric constructs, and site-directed mutagenesis

The full-length cDNA encoding mouse TRPM8 in pcDNA5 and chicken TRPM8 in pcDNA3 were kindly provided by Drs. Ardem Patapoutian and David Julius, respectively. TRPM8 chimeras and single-point mutants were obtained by overlap extension PCR. In all of these techniques we used *PfuUltra* polymerase (Agilent, Santa Clara, CA). The chimeric constructs were subcloned in pcDNA3.1/myc-His A (Thermo Fisher Scientific, Invitrogen). Before use, all constructs were verified by DNA sequencing (Macrogen, Seoul, South Korea).

Animals

This study was performed using young adult P21 C57BL6 mice and P10 Leghorn chickens. All experiments were conducted according to the bioethical guidelines of the *Comisión Nacional de investigación Científica y Tecnológica de Chile* (CONICYT) and have been approved by the Bioethical Committee of the University of Santiago de Chile (Reference Number 533).

Cell culture and transfection

HEK293 cells were plated in 24-well dishes at 1×10^5 cells/well, and transiently transfected with 1 μg of indicated DNA and Lipofectamine 2000 (Thermo Fisher), following the manufacturer's indications. At 48 h posttransfection, calcium imaging experiments were performed. DRG neurons from mice and chickens were cultured as previously described (40, 44). Briefly, the DRGs were isolated and disaggregated in 1 mg/ml collagenase type 1A and cultured in Dulbecco's modified Eagle's medium/F-12 mixture, containing 10% fetal bovine serum (Thermo Fisher) and supplemented with 4 mM L-glutamine (Thermo Fisher), 17 mM glucose, nerve growth factor (mouse 7S, 100 ng/ml; Merck, Sigma-Aldrich), and antibiotics. Cells were plated on polysine-coated glass coverslips and used during the following 24 h.

Western blotting

HEK293 cells were transiently transfected with TRPM8 constructs for 48 h. Equal amounts of protein for each condition (15–30 μg) were loaded onto a 7.5% SDS-polyacrylamide gel and electrophoresed. Proteins were transferred to a nitrocellulose membrane, blocked with 10% skim milk in PBS, and incubated with antibodies against the Myc epitope and GAPDH (Merck, Sigma-Aldrich), diluted to 1:3000 and 1:10,000, respectively, in PBS with Tween 20. HRP-coupled anti-rabbit secondary antibodies (Merck, Sigma-Aldrich) were used at a final concentration of 1:2000 for detection, and the signal was detected with a SuperSignal West Pico Chemiluminescent kit (Thermo Fisher).

Ca^{2+} imaging

HEK293 cells cotransfected for 48 h with 1 μg of TRPM8 construct and 0.25 μg of a fluorescent reporter were loaded with 5 μM Fura-2AM (Invitrogen) in standard extracellular solution (in mM): 140 NaCl, 3 KCl, 1.3 $MgCl_2$, 2.4 $CaCl_2$, 10 glucose, and 10 HEPES, pH 7.4 adjusted with NaOH (297 mOsm/kg) supplemented with 0.02% Pluronic (Thermo Fisher, Invitrogen) for 45 min at 37 °C in the dark. Fluorescence measurements were performed with an inverted Nikon Eclipse Ti-U microscope fitted with a 12-bit cooled ORCA C8484–03G02 CCD camera (Hamamatsu, Hamamatsu City, Japan). Fura-2 was excited at 340 nm and 380 nm with a Polychrome V monochromator (Thermo Fisher, Till Photonics), with exposure times of 30 ms, and the emitted fluorescence was filtered with a 510 nm long-pass filter. Calibrated ratios sampled every 2 s were displayed online with HCImage v1.2 software (Hamamatsu). In our experimental conditions using Fura-2, estimated mean cold- and menthol-evoked Ca^{2+} increases induced by TRPM8 activation in both sensory neurons and mTRPM8-transfected HEK293 cells are between 200 and 450 nM (38–40, 43, 44), a $[Ca^{2+}]_i$ still distant from the saturation of the probe. Bath temperature (see below for details) was recorded simultaneously with an IT-18 Type T thermocouple connected to a Physitemp BAT-12 microprobe thermometer (Physitemp Instruments, Clifton, NJ) and digitized with an AD converter running Clampex 10 software (Molecular Devices, Sunnyvale, CA). Threshold temperature values for $[Ca^{2+}]_i$ elevation were estimated by interpolating the temperature at the midpoint between the last baseline point and the first point at which a rise in $[Ca^{2+}]_i$ was deviated by at least four times the S.D. of the baseline.

Electrophysiological recordings

Whole-cell voltage clamp recordings in transfected HEK293 cells were performed simultaneously with temperature recordings. Standard patch pipettes (3–5 megohms) were made of borosilicate glass capillaries (Harvard Apparatus Ltd, Cambridge, UK) and contained (in mM): 130 CsCl, 1 EGTA, 10 HEPES, 4 ATP-Mg, and 0.4 GTP-Na, pH adjusted to 7.4 with CsOH (280 mOsm/kg). The bath solution was the same as that used in the calcium imaging experiments. Current signals were recorded with an Axopatch 200B patch clamp amplifier (Molecular Devices). Stimulus delivery and data acquisition were performed using pCLAMP10 software (Molecular Devices). To estimate the shifts in the voltage-dependent activation of TRPM8, current–voltage (I–V) relationships obtained from repetitive (0.2 Hz) voltage ramps (−100 to +180 mV, with a slope of 200 mV/s) were fitted with a function that combines a linear conductance multiplied by a Boltzmann activation term (41),

$$I = g \times (V - E_{rev})/(1 + \exp((V_{1/2} - V)/s)) \qquad \text{(Eq. 1)}$$

where g is the whole-cell conductance, E_{rev} is the reversal potential of the current, $V_{1/2}$ is the potential for half-maximal activation, and s is the slope factor. The assumption of a linear conductance is based on a previous observation by Voets *et al.* (12) that when the TRPM8 channel opens it exhibits ohmic I–V dependence. Q_{10} was obtained from the slope of a log(I) *versus* T plot or by directly fitting the data using Equation 2,

$$Q_{10} = (I_2/I_1)\exp(10/(T_2 - T_1)) \qquad \text{(Eq. 2)}$$

where I_1 and I_2 are the measured currents at temperatures T_1 and T_2, respectively.

Temperature stimulation

Coverslips with cultured cells were placed in a microchamber and continuously perfused with solutions warmed to ~34 °C. The temperature was adjusted with a water-cooled computer-controlled Peltier device placed at the inlet of the recording chamber and controlled by a feedback device. Cold sensitivity was investigated with temperature drops from 34 to 18 °C.

Variance analysis

To estimate the number of mM8-myc and 507–556 channels in the plasma membrane, we used nonstationary noise analysis (13, 48). 100 current records in whole-cell configuration were collected for each cell during activation of the channels by 150 ms depolarizing voltage steps from 0 to +180 mV, at 19 °C. Ensemble averaged current ($\langle I \rangle$) and its variance (σ^2) on each isochrone were calculated. The variance as a function of $\langle I \rangle$ was fitted using Equation 3,

$$\sigma^2 = i^*\langle I \rangle - (\langle I \rangle^2/N) \quad \text{(Eq. 3)}$$

where i is the single channel unitary current and N is the number of channels in the plasma membrane. The maximum open probability (P_o max) was estimated using the relation $P_o\,\text{max} = I_{max}/i^*N$, where I_{max} is the mean maximal current in each experiment. Data for variance analysis were acquired at 20 kHz and filtered at 5 kHz.

Data analysis

Data are reported as scatter plots that show all the individual values and S.D. to represent variation, and as mean ± S.E., from n cells studied. For all relevant questions addressed here, at least 3 independent days of experiments were carried out. When comparing two mean values, statistical significance ($p < 0.05$) was assessed using Student's unpaired, two-tailed t test. For multiple comparisons of means, one-way analysis of variance (ANOVA) was performed in combination with a Bonferroni's or Dunnett's post hoc test. Data analysis was performed using Prism 5 (GraphPad Software).

Author contributions—M. P. conceptualization; M. P. and R. M. resources; M. P., B. R., A. G., G. U., and R. M. formal analysis; M. P. and R. M. supervision; M. P. and R. M. funding acquisition; M. P., B. R., A. G., G. U., and R. M. investigation; M. P. and R. M. methodology; M. P. writing-original draft; M. P. and R. M. project administration; M. P., B. R., A. G., G. U., and R. M. writing-review and editing.

Acknowledgments—We thank Dr. Félix Viana for providing comments on the manuscript. We thank R. Pino, K. Tralma, J. Salas, and M. Campos for the excellent technical assistance.

References

1. Heppelmann, B., Messlinger, K., Neiss, W. F., and Schmidt, R. F. (1990) Ultrastructural three-dimensional reconstruction of group III and group IV sensory nerve endings ("free nerve endings") in the knee joint capsule of the cat: Evidence for multiple receptive sites. *J. Comp. Neurol.* **292,** 103–116 CrossRef Medline
2. Hensel, H., and Zotterman, Y. (1951) The effect of menthol on the thermoreceptors. *Acta Physiol. Scand.* **24,** 27–34 CrossRef Medline
3. Iriuchijima, J., and Zotterman, Y. (1960) The specificity of afferent cutaneous C fibres in mammals. *Acta Physiol. Scand.* **49,** 267–278 CrossRef Medline
4. Colburn, R. W., Lubin, M. L., Stone, D. J., Jr., Wang, Y., Lawrence, D., D'Andrea, M. R., Brandt, M. R., Liu, Y., Flores, C. M., and Qin, N. (2007) Attenuated cold sensitivity in TRPM8 null mice. *Neuron* **54,** 379–386 CrossRef Medline
5. Dhaka, A., Murray, A. N., Mathur, J., Earley, T. J., Petrus, M. J., and Patapoutian, A. (2007) TRPM8 is required for cold sensation in mice. *Neuron* **54,** 371–378 CrossRef Medline
6. Bautista, D. M., Siemens, J., Glazer, J. M., Tsuruda, P. R., Basbaum, A. I., Stucky, C. L., Jordt, S.-E., and Julius, D. (2007) The menthol receptor TRPM8 is the principal detector of environmental cold. *Nature* **448,** 204–208 CrossRef Medline
7. Pertusa, M., Moldenhauer, H., Brauchi, S., Latorre, R., Madrid, R., and Orio, P. (2012) Mutagenesis and temperature-sensitive little machines. in *Mutagenesis*, pp. 221–246, InTech Open, London, United Kingdom
8. Vay, L., Gu, C., and McNaughton, P. A. (2012) The thermo-TRP ion channel family: Properties and therapeutic implications. *Br. J. Pharmacol.* **165,** 787–801 CrossRef Medline
9. Islas, L. D. (2017) Molecular mechanisms of temperature gating in TRP channels. in *Neurobiology of TRP Channels* (Rosembaum, T., ed), pp. 20–31, CRC Press/Taylor & Francis, Boca Ratón, FL
10. Peier, A. M., Moqrich, A., Hergarden, A. C., Reeve, A. J., Andersson, D. A., Story, G. M., Earley, T. J., Dragoni, I., McIntyre, P., Bevan, S., and Patapoutian, A. (2002) A TRP channel that senses cold stimuli and menthol. *Cell.* **108,** 705–715 CrossRef Medline
11. McKemy, D. D., Neuhausser, W. M., and Julius, D. (2002) Identification of a cold receptor reveals a general role for TRP channels in thermosensation. *Nature* **416,** 52–58 CrossRef Medline
12. Voets, T., Droogmans, G., Wissenbach, U., Janssens, A., Flockerzi, V., and Nilius, B. (2004) The principle of temperature-dependent gating in cold- and heat-sensitive TRP channels. *Nature* **430,** 748–754 CrossRef Medline
13. Brauchi, S., Orio, P., and Latorre, R. (2004) Clues to understanding cold sensation: Thermodynamics and electrophysiological analysis of the cold receptor TRPM8. *Proc. Natl. Acad. Sci.* **101,** 15494–15499 CrossRef Medline
14. Raddatz, N., Castillo, J. P., Gonzalez, C., Alvarez, O., and Latorre, R. (2014) Temperature and voltage coupling to channel opening in transient receptor potential melastatin 8 (TRPM8). *J. Biol. Chem.* **289,** 35438–35454 CrossRef Medline
15. Almaraz, L., Manenschijn, J.-A., de la Peña, E., and Viana, F. (2014) TRPM8. *Handb. Exp. Pharmacol.* **222,** 547–579 CrossRef Medline
16. Madrid, R., and Pertusa, M. (2014) Intimacies and physiological role of the polymodal cold-sensitive ion channel TRPM8. *Curr. Top. Membr.* **74,** 293–324 CrossRef Medline
17. Pérez de Vega, M. J., Gómez-Monterrey, I., Ferrer-Montiel, A., and González-Muñiz, R. (2016) Transient receptor potential melastatin 8 channel (TRPM8) modulation: Cool entryway for treating pain and cancer. *J. Med. Chem.* **59,** 10006–10029 CrossRef Medline
18. Tsuruda, P. R., Julius, D., and Minor, D. L., Jr. (2006) Coiled coils direct assembly of a cold-activated TRP channel. *Neuron* **51,** 201–212 CrossRef Medline
19. Stewart, A. P., Egressy, K., Lim, A., and Edwardson, J. M. (2010) AFM imaging reveals the tetrameric structure of the TRPM8 channel. *Biochem. Biophys. Res. Commun.* **394,** 383–386 CrossRef Medline
20. Janssens, A., and Voets, T. (2011) Ligand stoichiometry of the cold- and menthol-activated channel TRPM8. *J. Physiol.* **589,** 4827–4835 CrossRef Medline
21. Yin, Y., Wu, M., Zubcevic, L., Borschel, W. F., Lander, G. C., and Lee, S.-Y. (2018) Structure of the cold- and menthol-sensing ion channel TRPM8. *Science* **359,** 237–241 CrossRef Medline
22. Bandell, M., Dubin, A. E., Petrus, M. J., Orth, A., Mathur, J., Hwang, S. W., and Patapoutian, A. (2006) High-throughput random mutagenesis screen reveals TRPM8 residues specifically required for activation by menthol. *Nat. Neurosci.* **9,** 493–500 CrossRef Medline
23. Malkia, A., Pertusa, M., Fernández-Ballester, G., Ferrer-Montiel, A., and Viana, F. (2009) Differential role of the menthol-binding residue Y745 in

the antagonism of thermally gated TRPM8 channels. *Mol. Pain* **5,** 62 CrossRef Medline
24. Chuang, H. H., Neuhausser, W. M., and Julius, D. (2004) The super-cooling agent icilin reveals a mechanism of coincidence detection by a temperature-sensitive TRP channel. *Neuron* **43,** 859–869 CrossRef Medline
25. Voets, T., Owsianik, G., Janssens, A., Talavera, K., and Nilius, B. (2007) TRPM8 voltage sensor mutants reveal a mechanism for integrating thermal and chemical stimuli. *Nat. Chem. Biol.* **3,** 174–182 CrossRef Medline
26. Brauchi, S., Orta, G., Salazar, M., Rosenmann, E., and Latorre, R. (2006) A hot-sensing cold receptor: C-terminal domain determines thermosensation in transient receptor potential channels. *J. Neurosci.* **26,** 4835–4840 CrossRef Medline
27. Brauchi, S., Orta, G., Mascayano, C., Salazar, M., Raddatz, N., Urbina, H., Rosenmann, E., Gonzalez-Nilo, F., and Latorre, R. (2007) Dissection of the components for PIP2 activation and thermosensation in TRP channels. *Proc. Natl. Acad. Sci. U.S.A.* **104,** 10246–10251 CrossRef Medline
28. Matos-Cruz, V., Schneider, E. R., Mastrotto, M., Merriman, D. K., Bagriantsev, S. N., and Gracheva, E. O. (2017) Molecular prerequisites for diminished cold sensitivity in ground squirrels and hamsters. *Cell Rep.* **21,** 3329–3337 CrossRef Medline
29. Pertusa, M., González, A., Hardy, P., Madrid, R., and Viana, F. (2014) Bidirectional modulation of thermal and chemical sensitivity of TRPM8 channels by the initial region of the N-terminal domain. *J. Biol. Chem.* **289,** 21828–21843 CrossRef Medline
30. Cordero-Morales, J. F., Gracheva, E. O., and Julius, D. (2011) Cytoplasmic ankyrin repeats of transient receptor potential A1 (TRPA1) dictate sensitivity to thermal and chemical stimuli. *Proc. Natl. Acad. Sci. U.S.A.* **108,** E1184–E1191 CrossRef Medline
31. Kang, K., Panzano, V. C., Chang, E. C., Ni, L., Dainis, A. M., Jenkins, A. M., Regna, K., Muskavitch, M. A. T., and Garrity, P. A. (2011) Modulation of TRPA1 thermal sensitivity enables sensory discrimination in *Drosophila*. *Nature* **481,** 76–80 CrossRef Medline
32. Chen, J., Kang, D., Xu, J., Lake, M., Hogan, J. O., Sun, C., Walter, K., Yao, B., and Kim, D. (2013) Species differences and molecular determinant of TRPA1 cold sensitivity. *Nat. Commun.* **4,** 1–7 CrossRef Medline
33. Laursen, W. J., Schneider, E. R., Merriman, D. K., Bagriantsev, S. N., and Gracheva, E. O. (2016) Low-cost functional plasticity of TRPV1 supports heat tolerance in squirrels and camels. *Proc. Natl. Acad. Sci. U.S.A.* **113,** 11342–11347 CrossRef Medline
34. Saito, S., Banzawa, N., Fukuta, N., Saito, C. T., Takahashi, K., Imagawa, T., Ohta, T., and Tominaga, M. (2014) Heat and noxious chemical sensor, chicken TRPA1, as a target of bird repellents and identification of its structural determinants by multispecies functional comparison. *Mol. Biol. Evol.* **31,** 708–722 CrossRef Medline
35. Saito, S., Ohkita, M., Saito, C. T., Takahashi, K., Tominaga, M., and Ohta, T. (2016) Evolution of heat sensors drove shifts in thermosensation between *Xenopus* species adapted to different thermal niches. *J. Biol. Chem.* **291,** 11446–11459 CrossRef Medline
36. Saito, S., and Shingai, R. (2006) Evolution of thermoTRP ion channel homologs in vertebrates. *Physiol. Genomics* **27,** 219–230 CrossRef Medline
37. Myers, B. R., Sigal, Y. M., and Julius, D. (2009) Evolution of thermal response properties in a cold-activated TRP channel. *PLoS One* **4,** e5741 CrossRef Medline
38. Mälkiä, A., Madrid, R., Meseguer, V., de la Peña, E., Valero, M., Belmonte, C., and Viana, F. (2007) Bidirectional shifts of TRPM8 channel gating by temperature and chemical agents modulate the cold sensitivity of mammalian thermoreceptors. *J. Physiol.* **581,** 155–174 CrossRef Medline
39. Pertusa, M., Madrid, R., Morenilla-Palao, C., Belmonte, C., and Viana, F. (2012) N-glycosylation of TRPM8 ion channels modulates temperature sensitivity of cold thermoreceptor neurons. *J. Biol. Chem.* **287,** 18218–18229 CrossRef Medline
40. Madrid, R., Donovan-Rodríguez, T., Meseguer, V., Acosta, M. C., Belmonte, C., and Viana, F. (2006) Contribution of TRPM8 channels to cold transduction in primary sensory neurons and peripheral nerve terminals. *J. Neurosci.* **26,** 12512–12525 CrossRef Medline
41. Nilius, B., Mahieu, F., Prenen, J., Janssens, A., Owsianik, G., Vennekens, R., and Voets, T. (2006) The Ca^{2+}-activated cation channel TRPM4 is regulated by phosphatidylinositol 4,5-biphosphate. *EMBO J.* **25,** 467–478 CrossRef Medline
42. Yamamoto, A., Takahashi, K., Saito, S., Tominaga, M., and Ohta, T. (2016) Two different avian cold-sensitive sensory neurons: Transient receptor potential melastatin 8 (TRPM8)-dependent and -independent activation mechanisms. *Neuropharmacology* **111,** 130–141 CrossRef Medline
43. González, A., Ugarte, G., Restrepo, C., Herrera, G., Piña, R., Gómez-Sánchez, J. A., Pertusa, M., Orio, P., and Madrid, R. (2017) Role of the excitability brake potassium current IKD in cold allodynia induced by chronic peripheral nerve injury. *J. Neurosci.* **37,** 3109–3126 CrossRef Medline
44. Madrid, R., de la Peña, E., Donovan-Rodriguez, T., Belmonte, C., and Viana, F. (2009) Variable threshold of trigeminal cold-thermosensitive neurons is determined by a balance between TRPM8 and Kv1 potassium channels. *J. Neurosci.* **29,** 3120–3131 CrossRef Medline
45. Bödding, M., Wissenbach, U., and Flockerzi, V. (2007) Characterisation of TRPM8 as a pharmacophore receptor. *Cell Calcium* **42,** 618–628 CrossRef Medline
46. Phelps, C. B., and Gaudet, R. (2007) The role of the N terminus and transmembrane domain of TRPM8 in channel localization and tetramerization. *J. Biol. Chem.* **282,** 36474–36480 CrossRef Medline
47. Bavencoffe, A., Gkika, D., Kondratskyi, A., Beck, B., Borowiec, A.-S., Bidaux, G., Busserolles, J., Eschalier, A., Shuba, Y., Skryma, R., and Prevarskaya, N. (2010) The transient receptor potential channel TRPM8 is inhibited via the α2A adrenoreceptor signaling pathway. *J. Biol. Chem.* **285,** 9410–9419 CrossRef Medline
48. Alvarez, O., Gonzalez, C., and Latorre, R. (2002) Counting channels: A tutorial guide on ion channel fluctuation analysis. *Adv. Physiol. Educ.* **26,** 327–341 CrossRef Medline
49. Grandl, J., Kim, S. E., Uzzell, V., Bursulaya, B., Petrus, M., Bandell, M., and Patapoutian, A. (2010) Temperature-induced opening of TRPV1 ion channel is stabilized by the pore domain. *Nat. Neurosci.* **13,** 708–714 CrossRef Medline
50. Grandl, J., Hu, H., Bandell, M., Bursulaya, B., Schmidt, M., Petrus, M., and Patapoutian, A. (2008) Pore region of TRPV3 ion channel is specifically required for heat activation. *Nat. Neurosci.* **11,** 1007–1013 CrossRef Medline
51. Jabba, S., Goyal, R., Sosa-Pagán, J. O., Moldenhauer, H., Wu, J., Kalmeta, B., Bandell, M., Latorre, R., Patapoutian, A., and Grandl, J. (2014) Directionality of temperature activation in mouse TRPA1 ion channel can be inverted by single-point mutations in ankyrin repeat six. *Neuron* **82,** 1017–1031 CrossRef Medline
52. Carrasquel-Ursulaez, W., Moldenhauer, H., Castillo, J. P., Latorre, R., and Alvarez, O. (2015) Biophysical analysis of thermosensitive TRP channels with a special focus on the cold receptor TRPM8. *Temperature* **2,** 188–200 CrossRef Medline
53. Clapham, D. E., and Miller, C. (2011) A thermodynamic framework for understanding temperature sensing by transient receptor potential (TRP) channels. *Proc. Natl. Acad. Sci. U.S.A.* **108,** 19492–19497 CrossRef Medline
54. Chowdhury, S., Jarecki, B. W., and Chanda, B. (2014) A molecular framework for temperature-dependent gating of ion channels. *Cell* **158,** 1148–1158 CrossRef Medline
55. Yao, J., Liu, B., and Qin, F. (2011) Modular thermal sensors in temperature-gated transient receptor potential (TRP) channels. *Proc. Natl. Acad. Sci. U.S.A.* **108,** 11109–11114 CrossRef Medline
56. Zhong, L., Bellemer, A., Yan, H., Ken, H., Jessica, R., Hwang, R. Y., Pitt, G. S., and Tracey, W. D. (2012) Thermosensory and nonthermosensory isoforms of *Drosophila* melanogaster TRPA1 reveal heat-sensor domains of a thermoTRP Channel. *Cell Rep.* **1,** 43–55 CrossRef Medline
57. Wang, H., Schupp, M., Zurborg, S., and Heppenstall, P. A. (2013) Residues in the pore region of *Drosophila* transient receptor potential A1 dictate sensitivity to thermal stimuli. *J. Physiol.* **591,** 185–201 CrossRef Medline
58. Cui, Y., Yang, F., Cao, X., Yarov-Yarovoy, V., Wang, K., and Zheng, J. (2012) Selective disruption of high sensitivity heat activation but not capsaicin activation of TRPV1 channels by pore turret mutations. *J. Gen. Physiol.* **139,** 273–283 CrossRef Medline

59. Owsianik, G., Talavera, K., Voets, T., and Nilius, B. (2006) Permeation and selectivity of TRP channels. *Annu. Rev. Physiol.* **68,** 685–717 CrossRef Medline
60. Bidaux, G., Sgobba, M., Lemonnier, L., Borowiec, A. S., Noyer, L., Jovanovic, S., Zholos, A. V., and Haider, S. (2015) Functional and modeling studies of the transmembrane region of the TRPM8 channel. *Biophys. J.* **109,** 1840–1851 CrossRef Medline
61. Erler, I., Al-Ansary, D. M. M., Wissenbach, U., Wagner, T. F. J., Flockerzi, V., and Niemeyer, B. A. (2006) Trafficking and assembly of the cold-sensitive TRPM8 channel. *J. Biol. Chem.* **281,** 38396–38404 CrossRef Medline
62. Dragoni, I., Guida, E., and McIntyre, P. (2006) The cold and menthol receptor TRPM8 contains a functionally important double cysteine motif. *J. Biol. Chem.* **281,** 37353–37360 CrossRef Medline
63. Yang, F., Cui, Y., Wang, K., and Zheng, J. (2010) Thermosensitive TRP channel pore turret is part of the temperature activation pathway. *Proc. Natl. Acad. Sci. U.S.A.* **107,** 7083–7088 CrossRef Medline
64. Kim, S. E., Patapoutian, A., and Grandl, J. (2013) Single residues in the outer pore of TRPV1 and TRPV3 have temperature-dependent conformations. *PLoS One* **8,** e59593 CrossRef Medline
65. Liao, M., Cao, E., Julius, D., and Cheng, Y. (2013) Structure of the TRPV1 ion channel determined by electron cryo-microscopy. *Nature* **504,** 107–112 CrossRef Medline
66. Cao, E., Liao, M., Cheng, Y., and Julius, D. (2013) TRPV1 structures in distinct conformations reveal activation mechanisms. *Nature* **504,** 113–118 CrossRef Medline
67. Hirschi, M., Herzik, M. A., Jr., Wie, J., Suo, Y., Borschel, W. F., Ren, D., Lander, G. C., and Lee, S.-Y. (2017) Cryo-electron microscopy structure of the lysosomal calcium-permeable channel TRPML3. *Nature* **550,** 411–414 CrossRef Medline
68. Andersson, D. A., Chase, H. W. N., and Bevan, S. (2004) TRPM8 activation by menthol, icilin, and cold is differentially modulated by intracellular pH. *J. Neurosci.* **24,** 5364–5369 CrossRef Medline
69. Fleig, A., and Penner, R. (2004) The TRPM ion channel subfamily: Molecular, biophysical and functional features. *Trends Pharmacol. Sci.* **25,** 633–639 CrossRef Medline
70. de la Peña, E., Mälkiä, A., Cabedo, H., Belmonte, C., and Viana, F. (2005) The contribution of TRPM8 channels to cold sensing in mammalian neurones. *J. Physiol.* **567,** 415–426 CrossRef Medline
71. Viana, F., de la Peña, E., and Belmonte, C. (2002) Specificity of cold thermotransduction is determined by differential ionic channel expression. *Nat. Neurosci.* **5,** 254–260 CrossRef Medline
72. Vriens, J., Nilius, B., and Voets, T. (2014) Peripheral thermosensation in mammals. *Nat. Rev. Neurosci.* **15,** 573–589 CrossRef Medline
73. McKemy, D. D. (2013) The molecular and cellular basis of cold sensation. *ACS Chem. Neurosci.* **4,** 238–247 CrossRef Medline
74. González, A., Ugarte, G., Piña, R., Pertusa, M., and Madrid, R. (2015) TRP channels in cold transduction. in *TRP Channels in Sensory Transduction*, pp. 185–207, Springer International Publishing, Heidelberg, Germany
75. Morin, C., and Bushnell, M. C. (1998) Temporal and qualitative properties of cold pain and heat pain: A psychophysical study. *Pain* **74,** 67–73 CrossRef Medline
76. Thompson, J. D., Higgins, D. G., and Gibson, T. J. (1994) CLUSTAL W: Improving the sensitivity of progressive multiple sequence alignment through sequence weighting, position-specific gap penalties and weight matrix choice. *Nucleic Acids Res.* **22,** 4673–4680 CrossRef Medline
77. Waterhouse, A. M., Procter, J. B., Martin, D. M. A., Clamp, M., and Barton, G. J. (2009) Jalview Version 2-A multiple sequence alignment editor and analysis workbench. *Bioinformatics* **25,** 1189–1191 CrossRef Medline
78. Saitou, N., and Nei, M. (1987) The neighbor-joining method: A new method for reconstructing phylogenetic trees. *Mol. Biol. Evol.* **4,** 406–425 CrossRef Medline
79. Kumar, S., Stecher, G., and Tamura, K. (2016) MEGA7: Molecular Evolutionary Genetics Analysis version 7.0 for bigger datasets. *Mol. Biol. Evol.* **33,** 1870–1874 CrossRef Medline